Programmable Microparticle Scaffolds for Enhanced Diagnostic Devices

MaryJoe Kathryn Rice

Submitted to the faculty of Virginia Polytechnic Institute and State University in partial fulfillment for the degree of

Master of Science

In

Mechanical Engineering

Rafael V. Davalos, Chair

Warren C. Ruder

Bahareh Behkam

Rolf Mueller

April 25th, 2017
Blacksburg, Virginia

Keywords: Molecular mechanics, microrobotics, synthetic biology, cell free systems, microparticles, programmable scaffolds

Programmable Microparticle Scaffolds for Enhanced Diagnostic Devices

MaryJoe Kathryn Rice

Abstract

Microrobotics is an emerging discipline with the potential to radically affect fields ranging from medicine to environmental stewardship. Already, there have been remarkable breakthroughs; small scale robots have been made that can selectively traverse the gastrointestinal tract, and others have been built that can fly in a manner inspired from bees. However, there are still significant challenges in microrobotics, and it remains difficult to engineer reliable power sources, actuators, and sensors to create robust, modular designs at the microscale. The miniaturization of the robotic system makes design and efficiency of these components particularly difficult. However, biological systems demonstrate the key features of robotics – sensing, actuation, processing – and are remarkably complex at the microscale. As such, many researchers have turned to biology for inspiration and living robotic components. In our laboratory we have engineered an *Escherichia coli* (*E. coli*) capable of producing surface display proteins to either anchor the cells, bind to functionalized nanoparticles, or capture small molecules from the environment, all complex actuation features. Additionally, we have created a processing unit that can create signals based on biological components, yet is non-living. This thesis focuses on the characterization of the surface display E. Coli system and the creation of programmable microparticle scaffolds that may be controlled by biological circuitry. In particular, by leveraging the strong interaction between biotin and streptavidin, I have created programmable microparticle scaffolds capable of attenuating the intensity of a fluorescent response in response to perturbations in the local environmental conditions. We believe this is an excellent enabling technology to facilitate the creation of complex behaviors at the microscale and can be used as a processing unit for simple decision making on microrobots. We foresee this technology impacting disciplines from medical microrobotics to environmental sensing and remediation.

Programmable Microparticle Scaffolds for Enhanced Diagnostic Devices

MaryJoe Kathryn Rice

General Audience Abstract

Robots have integrated into industries ranging from car manufacturing to in-hospital transportation. However, recently there has become a new desire for robotics at a smaller scale, for use in fields ranging from medicine to agriculture. For example, how awesome would it be if we had small robots traveling through our bloodstream giving therapeutic drugs as needed or selectively killing tumor cells? This is the dream and goal of many research labs currently. However, when we try to design these tiny robots, we find that we are unable to use many of the normal components that are seen when looking at conventional electronics, AAA batteries as power sources for example. To build upon the example, how would a tiny robot in the body power itself or know when it has reached a cancerous tumor? We propose that the problem of decreased space can be solved by using biological components, like bacteria cells which already live at a microscopic scale, to power these robots and help them sense their surroundings. The work discussed in this thesis involves the design of biological sensors and processing units. We have proven that by engineering the DNA of bacteria cells, using the tools of synthetic biology, we are able to use the outside of the cell (cell's surface) to sense components in the environment. We hope that the findings discussed in this thesis will serve as the ground work for integrating living cells and robotics for future applications ranging from medicine to environmental remediation.

Acknowledgements

I would like to thank Dr. Warren Ruder for his patience, constant encouragement, and guidance throughout my degree. I could not have accomplished this without him. I additionally thank Dr. Rafael Davalos for his help and mentorship. Finally, I thank Dr. Bahareh Behkam and Dr. Rolf Mueller for their intellectual input.

To my family and friends, your support has meant the world to me throughout this degree. To my fellow colleagues, both old and new: Keith Heyde, Felicia Scott, Jack Lake, Sung-Ho Paek, Ruihua Zhang, Michael Behrens, Ming-Cheng Chang, and James Dulaney. Thank you for making my time in the lab not only manageable but also entertaining.

This work was supported primarily by awards N00014-17-12306 and N00014-15-1-2502 (to W.C.R.) from the Office of Naval Research. The author also acknowledges support from award FA9550-13-1-0108 from the Air Force Office of Scientific Research of the USA. Lastly, the author gratefully acknowledges graduate support from the Virginia Sea Grant Graduate Research Fellowship Program and the Virginia Tech Center for Innovation and Entrepreneurship.

Attribution

Several colleagues aided in the research and writing of two of the chapters in this thesis. A brief discussion of their contributions are listed here:

Chapter 3: Characterization of Engineered E. Coli bacteria with orthogonal protein expression between the cytosol and the surface

This work was conducted under the direction of Ph.D. student Felicia Y. Scott. While a Master's student in the Biological Systems Engineering Department at Virginia Tech, Felicia Scott engineered the surface display system that was characterized in Chapter 3 of this thesis. As a Ph.D. student in the same department and laboratory, she served as a mentor and aided in experimental design, analysis, and validation of the results.

Chapter 4: Modeling Information Exchange Between Artificial and Living Cells

Keith C. Heyde is a graduated Master's student from the Engineering Science and Mechanics department at Virginia Tech, now continuing with his Ph.D. at Carnegie Mellon University in Mechanical Engineering. He was a significant contributor to the work published in Chapter 4 of this thesis. Specifically, the work was based off of many previously published models that were designed by him. He helped significantly with the design of the new models and with the formatting of the figures in this chapter.

Table of Contents

List of Figures

List of Tables

Chapter I: Introduction

Background and Motivation

The ability to sense environmental information, process it, and react is ubiquitous in nature [1]. However, the recreation of these mechanisms in robotics is still a main research area, despite promising achievements. Many researchers and companies focus on the macroscale actuation and movement from humanoid hands [2] to bipedal walking [3]. These systems employ arrays of large sensors, actuators, and processing units that can aid robots in developing similar humanoid sensing and processing skills. However, the same toolkit of components is often not available at a smaller scale.

Microrobotics is an older discipline though many of its breakthrough technologies have been over the past decade. The technology has the power to impact fields from botany to medicine. Indeed, recently the National Science Foundation (NSF) has tasked roboticists with the challenge of creating flying microrobots capable of pollinating plants after an alarming decline in honeybee populations. Robert Wood's group at Harvard led the charge in creating "robobees" capable of flight, based on a biomimetic system [4, 5]. However, even the most advanced technologies are troubled by a lack of efficient, miniaturized components.

Though there have been large breakthroughs in microelectromechanical systems (MEMS) recently, we are still not able to sense and process with the same efficiency and speed as biological components. We therefore turn to the integration of biological components with microrobots for better control and processing. One key tool in this kit is synthetic biology, a proven field in the creation of multiple synthetic circuits and biosensors [6-9].

Research Objectives

Here, we have leveraged the tools of cell-free synthetic biology and programmable microparticle scaffolds to develop a technology to facilitate the creation of complex behaviors at the microscale. We envision this as an enabling system that can be used as a processing unit for simple decision making on microrobots. We accomplished this goal by completing the following objectives.

1. Use synthetic biology to explore spatially discretized options when working on a microscale
2. Explore the interactions between engineered cells, artificial protocells, and the biomolecular environment
3. Experimentally modulate fluorescent response using microparticle scaffolds and cell free synthetic biology

Thesis Organization

This thesis is organized into 6 informative chapters. The first chapter contains basic background on the thesis topic while the second chapter provides an in depth literature review of all relevant topics. The third chapter discusses the details of characterizing an orthogonal display system including background, previous results, methods, and dose response curves for a new synthetic circuit. The fourth chapter discusses modeling methods for cell free systems modulated by biotin producing cells while the fifth chapter presents experimental data to contrast with parts of the model. Lastly, the sixth chapter examines the impact of the work and future steps.

Chapter 2: Literature Review

Robotics

Robots entered the modern world as an industrial tool, first used in factories to automate production processes [10] but now are a staple in our homes [11], military [12, 13], medicine [14-16], and are quickly becoming integrated into evermore industries. One of the largest thrusts in robotics is the creation of autonomous robots. According to the International Organization for Standardization, robot autonomy is described as the ability to sense, process information, and perform tasks without human intervention [17]. Briefly, this requires robots to have sensors suitable for their environment, processing capabilities sufficient to deal with incoming sensory information, and a decision architecture in place to decide on an action based on the information supplied [18]. While there are many component options for large robots without intense space design constraints, the choices become scarce when moving to smaller and even microscale robotics.

Microrobotics and Microelectromechanical Systems

Over the past decade, there has been a drive to create small scale robots, often referred to as microrobots, capable of therapeutic drug delivery and improved diagnostic capabilities. The small size of the system presents a large design constraint on the sensors, actuators and processing units capable of being housed within the system that cannot be met with traditional methods. The field has therefore turned to microelectromechanical systems (MEMS). MEMS is not a new technology, and in fact since the 1980's the accelerometers in most cars' airbags are MEMS devices. However, with improved manufacturing methods and better control, we now have the ability to leverage MEMS technology, often around the size of a human hair, to recreate the autonomous capabilities at a microscale [19].

Microrobotics in medicine

One of the most widely used robots in medicine, other than surgical assist robots, is the capsule endoscopy for gastrointestinal (GI) diagnosis [20, 21]. The capsule is about the size of a pill and can be swallowed by a patient and travel through their gut before leaving the body with the feces. While inside the body, the capsule records movements and images as it travels from stomach to small intestine and through the GI tract. As the name suggests, the capsule endoscopy replaces a traditional endoscopy, an invasive and uncomfortable procedure for patients. The GI tract provides an optimum entry for intrabody robotics due to its relatively large size of a few millimeters [22]. The large size greatly reduces the risk for an obstruction causing harm to the patient. Additionally, the GI tract provides optimal entry (orally) and exit (with fecal waste) points for the device allowing simple injection and collection [23]. While each of these are important advantages that have contributed to the early and widespread adoption of the capsule endoscopy, the most important factor is that the robot does not have to move itself and is instead propelled forward by the natural peristalsis of the gut. While the capsule endoscopy has certainly been a ground breaking technology, in order to navigate smaller, and more complex systems of the body, our technology and systems will need to decrease in size as well.

Leveraging biological components as actuators on microrobots

Biology already provides micro and nano sized components capable of using biological components for power. It is therefore no surprise that many biomimetic technologies have been developed for microrobots. Additionally, the use of biological components as actuators for systems holds many developments.

One integration of a living/nonliving system was developed by Bahareh Behkam and relies on prokaryotic flagella to propel a small robot [24, 25]. This approach relies on bacteria attaching in

an end on arrangement to a polymer disk (Figure 1A,B). Once the bacteria are attached, they will be able to propel the robot using the rotation of their flagella. This served as a foundational technology allowing the development of modular systems. For instance, the body of the robot can be filled with multiple therapeutic drugs or substituted with a microparticle targeting a specific area. Additionally, the robot can be directed by natural processes [26] such as chemotaxis [27, 28], magnetotaxis [29], or phototaxis [30].

More recently, there has been a big push to create "living machines" led by Kit Parker, Rashid Bashir, and Roger Kamm [31-33]. In particular, Parker's group developed a biomimetic swimming skate created from gold, elastomer, and engineered cardiomyocytes (Figure 1C). Using cleverly patterned cardiomyocytes, the group was able to reconstruct the movement of a swimming skate using light activation. Furthermore, the skate was able to navigate an obstacle course suitable for its environment pointing to the tight level of directional control given by the design [34]. It should be noted that the skate requires researcher intervention in order to be guided in the desired direction. However, this serves as a breakthrough technology in functional hybrid robotics using biological components as actuators.

Synthetic biology

To engineer biological components to sense, actuate, or manipulate their environment, it is beneficial to employ the unique set of cellular programming tools provided by synthetic biology. In 2000, synthetic biology was launched with reports of two synthetic gene networks [6, 35], the "repressilator" and the "toggle switch." These two foundational systems used feedback control in order to provide increased complexity into engineered gene networks. Often referred to as synthetic gene circuits, these systems have rapidly advanced to include control structures such as counters, timers, and logic gates [36-38]. Furthermore, sophisticated algorithms and software tools

have been developed to assist in engineering biological networks [39, 40]. These research thrusts have built a foundation for synthetic biology as a complete discipline.

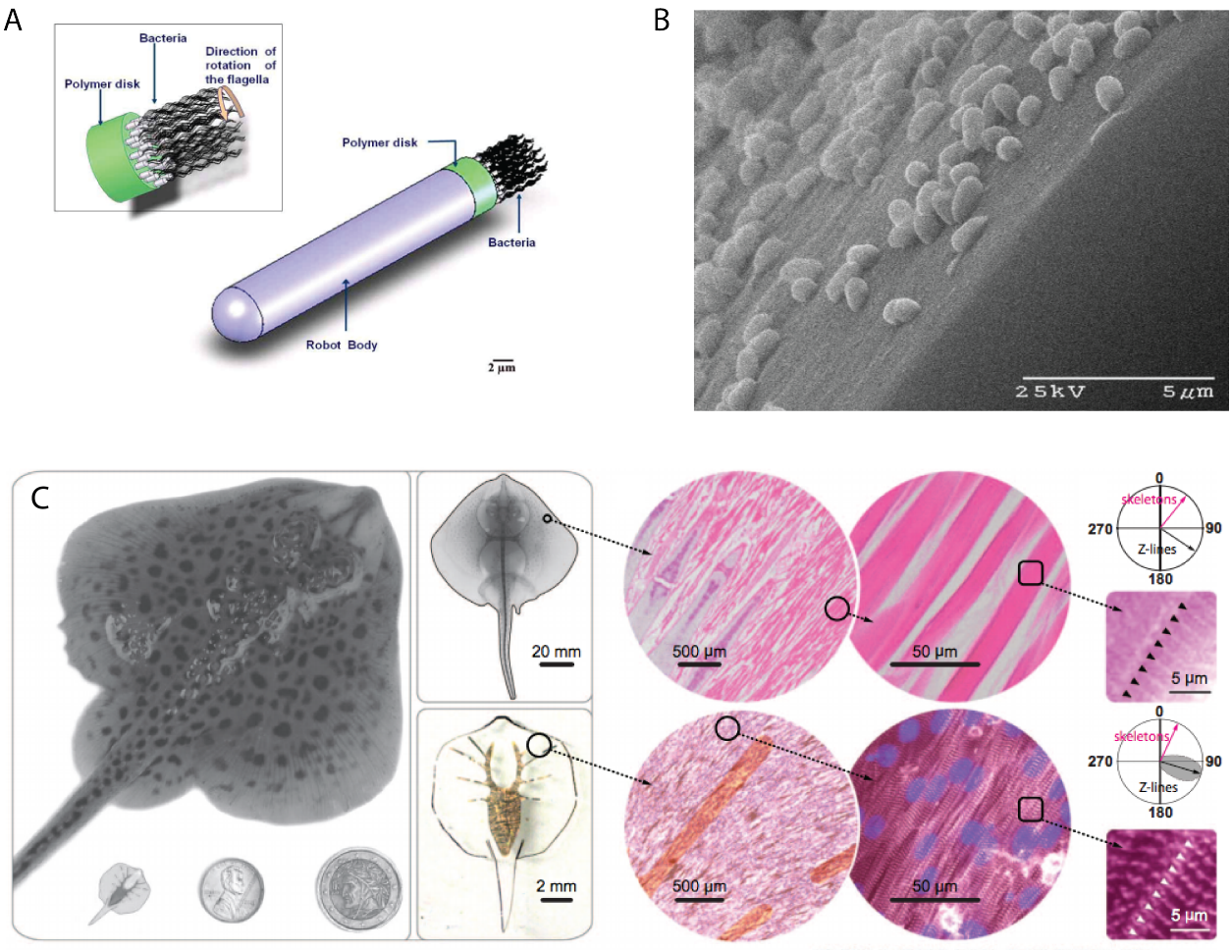

Figure 1: Using biological components as actuators for microrobots. A) The proposed robotic design of a flagella propelled robotic system [24], B) SEM image showing end on arrangement of bacteria on a polymer disk [25]. C) Hybrid system using engineered, light activated rat cardiomyocytes to actuate an underwater, biomimetic skate [34].

Whenever attempting to engineer materials, care should be taken to ensure robust design and synthesis processes, along with repeatable and precise structures. Biological systems naturally incorporate robust design and synthesis processes throughout their design. Reproducing these

systems by imitating them through biomimicry is a widely-used approach to capture the useful qualities of biological materials [41]. Yet, cells themselves hold potential as sensors, actuators, and processing units.

For example, since these foundational circuits of the toggle switch and repressilator were first reported, synthetic biology efforts have expanded on the potential for digital logic gate behavior in circuits [37, 42-44] using polymerases [37] as well as recombinases [45, 46]. In one case, Anderson et al. engineered a synthetic AND gate in bacteria (Figure 2a). In this circuit there are two inputs required to make a product. Input 2 produces transcription of an engineered viral RNA polymerase. However, this transcribed RNA has a small defect in it which is only fixed when the small RNA from Input 1 is also present. Therefore, with both inputs present we are given a functional viral RNA polymerase capable of transcribing our output signal (in this case green fluorescent protein). However if only one input is present we cannot transcribe the output signal and it is therefore not produced [37]. In a separate study by the Voigt group, they showed that communities of bacteria could work together to produce NOR-gate behavior [44], which is *Boolean complete*. Importantly, this means that it can be combined to form any other type of logic gate, thus suggesting that with cross talk between different bacterial populations, complex digital behavior could evolve. Of course, applications may also require analog signals, and work in the lab of Timothy Lu at MIT has recently shown that synthetic techniques can be applied to create sophisticated analog circuits in single bacteria cells [47].

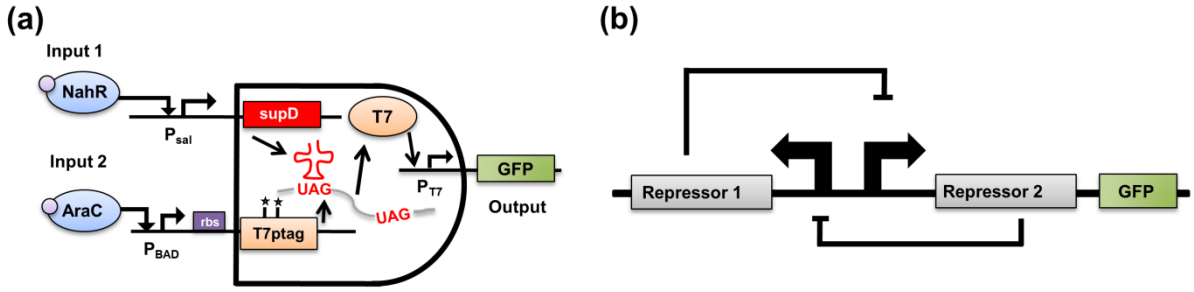

Figure 2 [48]. Synthetic gene circuits. (a) engineered AND logic gate [37] and (b) bistable "toggle" switch [6].

Both the digital and analog circuitry given by synthetic biology clearly allow for a small scale simple processing unit. Furthermore, most synthetic gene circuits signal using fluorescent protein reporters, such as mCherry (red) or green fluorescent protein (GFP). This allows for simple optical detection of response by the bacteria which can integrate into the decision making architecture of the microrobot. Better yet, as the average bacteria is about the size of one micron, a microrobot can easily house a colony of synthetically engineered E. coli capable of sensing and processing the environment around them.

Cell free systems

Cell free expression systems were first developed almost 60 years ago with a transcription only system in place, later followed by a transcription-translation (TX-TL) systems [49-51]. These systems exist for viral components, often using the T7 bacteriophage components, generally resulting in higher protein yield over a shorter period [52]. However, these systems are notably expensive and many labs therefore choose the cheaper option of bacterial based components despite the lower yield and longer reaction times. The bacterial based system has been optimized over many decades using S30A bacteria cells to make in house cell free expression [53-55]. Generally this method greatly reduces cost, in particular the system developed in Vincent Noireaux's lab claims a 98% cost reduction compared to viral systems [55].

The use of cell free systems can be extremely advantageous in synthetic biology. There are multiple advantages to using cell free systems in place of whole cell synthetic biology. Cell free systems include all of the components of the molecular building blocks in a cell without the cell wall. This is beneficial as it takes away the need for molecule transport across the cell wall and

negates the metabolic requirements of the cell. The result is a nanofactory of cellular components readily deployable for use without having to consider the cell's own objectives [56].

Furthermore, there are still breakthroughs in cell free systems developing with both Noireaux and Collins groups leading the charge. First, the development of freeze dried cell free (FD-CF) systems allows storage of components for up to a year [8] at low cost. Additionally, when combined with a toehold RNA switch sensor [7], it is possible to create low cost, portable sensors for detection of biological items such as the Zika virus [9]. Recently, the lab of Jim Collins has further expanded their expertise in the field to include not only on demand sensor production but portable vaccine production and biomanufacturing capabilities [57].

In this work we have leveraged synthetic biology's processing capabilities to create an enabling technology that can be used on microrobots in the future to aid in navigation of complex biological environments. Overall, a system has been developed using functionalized microparticle scaffolds to create a cell free synthetic biology processing unit.

Chapter 3: Characterization of engineered *E. Coli* bacteria with orthogonal protein expression between the cytosol and cell surface

Background

As synthetic biology continues to develop more gene circuits, there is a growing need to use multiple circuits simultaneously within a single organism. This parallel information processing is accomplished by engineering orthogonality into these gene circuits. However, cells are very small and face similar space constraints seen in microrobots, Eukaryotic cells have the benefit of spatially discretizing within their different membrane bound organelles within a single cell. However, bacteria cells are only few microns in length and do not have organelles, making spatial discretization within the cell much more difficult. To get around this issue, researchers have created synthetic spatial discretization. Of note are spatially separated microfluidic chips [58-60], and "chemical wires" connecting different cellular colonies [44].

Clearly, approaches to parallel information processing attempted thus far have heavily relied on either placing different gene circuits in spatially separated cell cultures [61, 62]. In our group, a new approach was developed by a graduate student, Felicia Scott, that leverages the outer cellular membrane (i.e., cellular envelope) to spatially separate synthetic outputs of an inducible synthetic circuit within a single prokaryote cell. In this chapter we will highlight her previous work [63] and then move into characterization results and future impact of the work.

Specifically, a system was developed for reporting synthetic circuit behavior based on bacterial surface-displayed fluorescent or enzymatic proteins. Normally, proteins produced inside the cell stay in the cytosol unless a transport mechanism exists to move them to the extracellular fluid. However, in this system we are able to anchor the protein of interest to the cell wall so that it displays to the extracellular space but is still attached to the cell. The bacteria used was *E. coli,* a gram-negative bacteria. Like all in its class, it has an outer membrane and a cytoplasmic membrane

separated by a small periplasmic space [64]. It should be noted that each of these membranes is the class phospholipid bilayer. With this known structure in mind, we designed and built synthetic components consisting of chimeric fusion proteins that could embed in the cellular envelope and reliably display functionally active proteins on the cell surface. We created two new fusion proteins based on lpp-ompA, allowing us to express mCherry, a red fluorescent protein reporter, and human O^6-alkylguanine DNA alkyltransferase (hAGT), also known as SNAP, on the surface of a bacterial cell.

The SNAP-tag was derived from O^6-alkylguanine-DNA-alkyltransferase (AGT), a human DNA repair enzyme [65]. AGT has a strong binding affinity for benzylguanine (BG) substituents [65]. The original AGT was then improved in 2006 [66] providing an optimized protein (SNAP) with a 50-fold increase in affinity for BG [66]. The SNAP-tag, because of its strong affinity and ease of attachment to any BG substituents, has since been widely utilized in a variety of studies ranging from medical applications, such as tumor targeting[67, 68] and drug delivery[69], to basic scientific research on protein network and interactions[70, 71]. Clearly, the SNAP tag is widely used across biotechnology applications. In fact, biotin and streptavidin (SA), known for having one of the strongest non covalent bindings in nature [72], are one of the only binding pairs that are used more. Though originally found in mammalian cells, SNAP has successfully been expressed in the bacterial cytosol [73]. However, since the report in 2010, there has been minimal development of the SNAP-tag technology in bacteria.

By fusing SNAP with the lpp-ompA protein, we created a line of *E. coli* with a strong, surface-displayed, BG-binding enzyme (Figure 3). The genetic construct endowed cells with a phenotypic expression platform orthogonal to traditional cytosolic fluorescent proteins. Additionally, the construct conferred an inducible ability that enabled cells to be selectively labelled by BG-

conjugated fluorescent chemical dyes while simultaneously upregulating intracellular fluorescent protein (i.e., mCherry) expression. As BG-conjugated dyes cannot be transported into the bacterial cytosol, this system confirmed that the SNAP enzyme was transported to the cell's surface while provideding a new method for selectivly discretizing surface and cytosolic features.

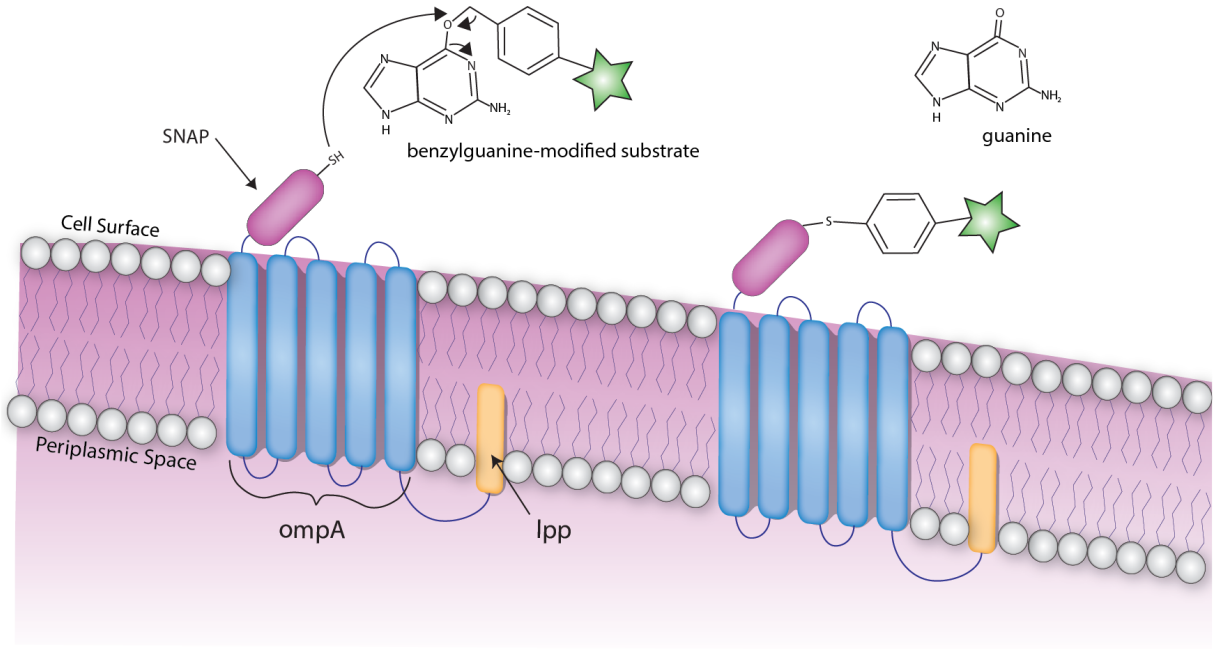

Figure 3: Schematic of fluorescent cell labelling of surface-displayed SNAP. The SNAP-tag® is displayed on the surface of E. coli by expression of an lpp-ompA-SNAP chimeric protein. The thiol group in the active site of the SNAP protein will react with the BG-modified substrate, resulting in the release of a guanine group and the covalent bonding of the substrate to the surface of the cell.

Previous Results [63]

The following highlights foundational work on the development of both surface displayed SNAP and mCherry proteins performed by Felicia Scott as part of her graduate degree [63].

Surface-displayed mCherry

In order to demonstrate the potential for cells to both properly translate, fold, assemble, and transport a fused protein-of-interest to the outer membrane of the cell, we designed a genetic

construct containing an mCherry encoding region behind an lpp-ompA sequence. The results showed that mCherry was expressed on the cell surface (Figure 4a-c). Using restriction enzyme cloning methods, the construct was developed by placing the *lpp-ompA* and *mCherry* sequences behind an arabinose inducible P_{BAD} promoter site in a plasmid containing an ampicillin resistance gene (Amp^R) for selective growth. Induction and dose response experiments were performed in K-12 *E. coli* strain MG1655 cells with the *araB*, *araA*, and *araD* genes knocked out [74] (*ΔaraBAD*). This knockout blocked the cell's ability to metabolize arabinose, while retaining arabinose's function as an inducer of the P_{BAD} promoter.

Using flow cytometry analysis, a clear shift in mCherry fluorescence was observed (Figure 4b). After data analysis, the shift in mean fluorescence between the uninduced (0% arabinose) and the induced (0.1% arabinose) cells was calculated to be significantly different with a p-value of < 0.0001 according to one-way ANOVA analysis and Student's t-test (Figure 4c). Standard deviation was calculated for each samples and is shown in the graphs in Figure 4c.

Surface-displayed SNAP

The mechanism of SNAP's function utilizes the covalent bonding of a BG-modified substrate to the thiol group in the active site of the SNAP protein. This bonding results in the release of a guanine group and the formation of a permanent covalent bond (Figure 3)[75], making the SNAP-system an ideal candidate for targeted molecular tagging.

The surface-displayed-SNAP plasmid was transformed into K-12 *E. coli* strain MG1655*ΔaraBAD* and induction studies were performed. After 6 hours of growth with arabinose, cells were labelled using SNAP- Cell® 505-Star fluorescent label (Figure 4d). SNAP-Cell® 505-Star was an ideal candidate for testing surface-displayed SNAP because the substrate excitation and emission spectra did not result in significant cross-talk with mCherry and the substrate binding was

restricted to the surface of the cells, eliminating any chance of labelling any SNAP proteins present in the cytosol. This inability for 505-star to enter the cell helped to confirm the localization of the SNAP-protein to the cell's surface. Induced cells demonstrated a statistically significant shift in labelling affinity, measured through flow cytometry with a p-value of < 0.0001 by ANOVA (Figure 4e-f). Standard deviation bars shown in Figure 4f.

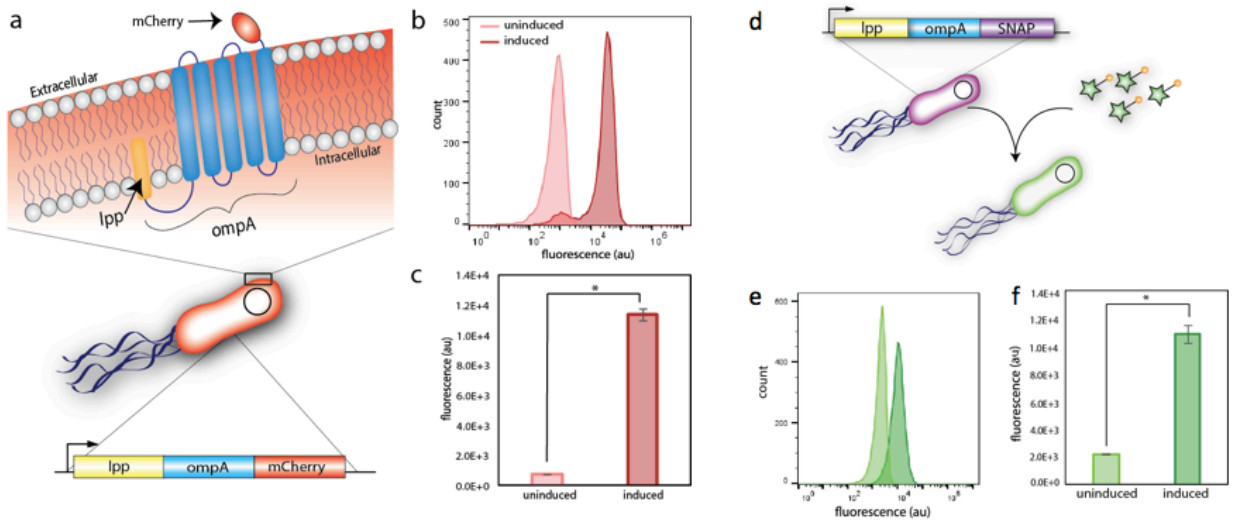

Figure 4: Development of a surface display technology in bacteria. The lpp-ompA fusion protein was used with (a-c) mCherry and (d-f) SNAP-tag. a) schematic representing the lpp-ompA protein expressing mCherry to the extracellular space. b-c) confirmation of proper induction of the synthetic circuit using flow cytometry (p-value: * < 0.0001, n = 3). d) surface display SNAP and labeling with SNAP-Cell® 505-Star to induce detectable green fluorescence e-f) confirmation of induction by labeling (p-value: * < 0.0001, n = 3) [63].

Materials and Methods

Media, reagents, growth

All *E. coli* cells were grown in Luria-Bertani (LB) Broth, Miller (Fisher Scientific). If an antibiotic was needed, the LB broth was allowed to cool to 55°C before antibiotic was added to a final concentration of 50 μg/mL.

Induction conditions and dose response curves

First, cells were grown for 6-8 hours and the OD_{600} of the cells was measured using a plate reader. If a value less than 0.8 was given, the following protocol was used. If a value greater than 0.8 was returned, the cells were diluted 1:1 in fresh LB media and allowed to grow for one hour before checking the OD_{600} again.

Following testing of the optical density to ensure exponential growth phase, the cells were aliquoted into 4 tubes with 400 μL each, one for each inducer concentration. Next the inducer concentrations were prepared in non-antibiotic LB media to a final concentration of 2x (for the control-0% simply have pure LB). 400 μL of each inducer concentration was then pipetted into the corresponding tube of cells effectively diluting the cells 1:1. 200 μL from each inducer tube was pipetted 3 separate times into different wells of a 96 well plate. The optical density was again checked to ensure the cells were between 0.2 and 0.8, or exponential growth phase. Following positive results, the first sample was measured on the flow cytometer with 10,000 events per sample.

The samples were then incubated at 37°C with agitation. Measurements were subsequently taken each hour for 6-8 hours. If fluorescent labeling was needed, a labeling sample was taken on each

hour while the population of cells stayed in the incubator with agitation to ensure proper growth conditions without stalling.

Data analysis was performed in SAS JMP Pro using mean fluorescence for each well.

Fluorescence Labelling

SNAP-Cell® 505-Star is a commercially available fluorescent tag (New England Biolabs, Inc.) with an excitation peak at 504 nm and an emission peak at 532 nm. mCherry has an excitation peak at 587 and an emission peak at 610. With no overlap in emission peaks, mCherry and SNAP-Cell® 505-Star should be easily distinguishable. Furthermore, the SNAP-Cell® 505-Star is a BG modified substituent and will only bind to SNAP proteins displayed on the outer membrane, as SNAP-Cell® 505-Star cannot cross the cell membrane thereby eliminating any chance of labeling proteins in the cytosol. The following procedure was developed in conjunction with the New England Biolabs, Inc.'s Cellular Labelling (S9103) protocol.

Before use, a 1 mM stock solution was created by adding 50 µL of DMSO was added to 50 nmol of labelling substrate. The solution was vortexed for 10 min before storing in a dark -20 °C freezer. Immediately before testing, the frozen stock was diluted 1:200, yielding a labelling medium of 5 µM dye substrate. The labelling medium was homogenized to reduce background by gentle, repetitive pipetting (10 times in the same vessel). 200 µL of cultured cells were resuspended in 30 µL of labelling medium by centrifuging cell cultures, removing the supernatant, and resuspending the cells by repetitive pipetting. The tubes were then incubated at 37 °C for 30 minutes. The cells were washed three times by centrifuging, decanting, and resuspending in 1X Phosphate Buffered Solution (PBS). Finally, the reactions were centrifuged and the supernatant was replaced a final time with PBS for further analysis in the flow cytometer.

Fluorescence Detection and Imaging

A Becton Dickinson Accuri™ C6 outfitted with a 488 nm laser and a 552 nm laser were used for all flow cytometry analysis. Further data processing was performed using FlowJo™ software. A Nikon eclipse Ti with an Andor® Zyla scientific CMOS (sCMOS) camera mounted for image acquisition was used for fluorescence imaging and Nikon's NIS-Elements software was used for capturing and analyzing images.

Results and Discussion

Orthogonal fluorescence in the cytosol and cell surface

To fully demonstrate orthogonal protein expression between the cytosol and cell surface, an mCherry gene was added to the existing surface display SNAP construct under control of a different promoter (Figure 5A). To demonstrate separate induction of both cytosolic and surface proteins, we replaced the constitutive promoter with a P_{BAD} promoter. Figure 5 shows the different induction schematics and the representative cell outputs.

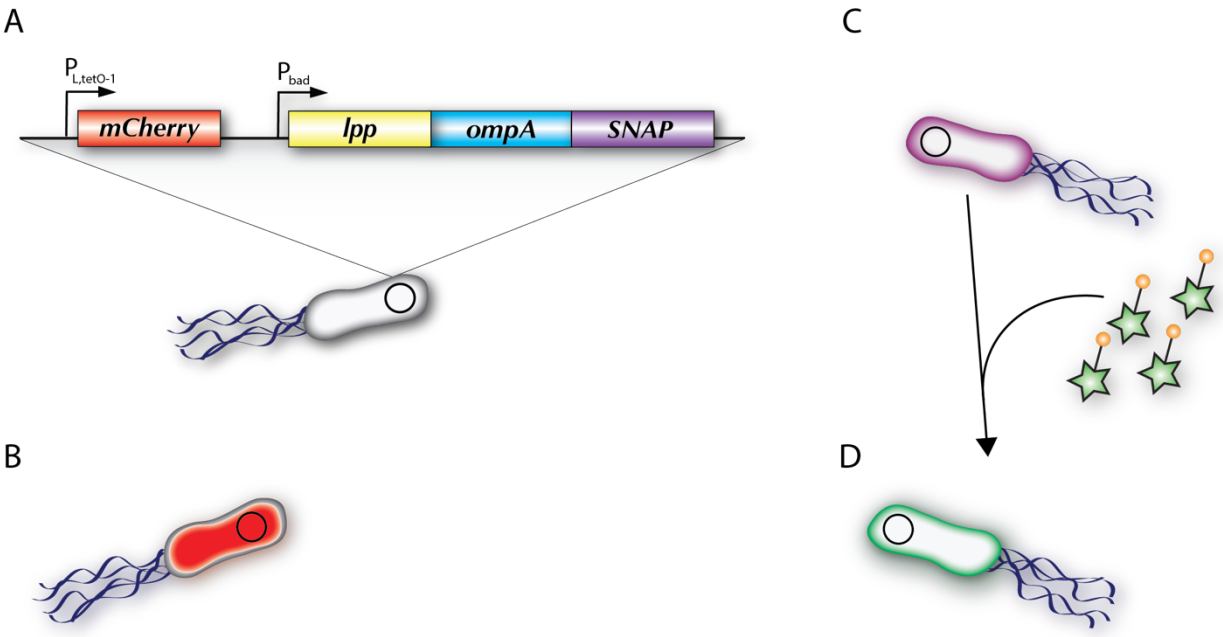

Figure 5: Characterization of orthogonal expression systems. A) Synthetic circuit with cytosolic mCherry inducible by aTc and surface displayed SNAP inducible by arabinose. B) Cell expressing cytosolic mCherry after aTc only induction. C) Cell expression of surface display SNAP after arabinose only induction. D) Cell representation after labeling with green fluorescent SNAP-Cell® 505-Star.

In order to test the orthogonality of the system, we ran two different tests. The first test was induction of only the mCherry circuit, with the use of aTc. We ran a dose response, with increasing concentrations of aTc from 0 to 0.5 μg/mL and measured the fluorescence output hourly. Furthermore, before measuring we labeled with SNAP-Cell® 505-Star. The labeling ensures that there is no leak in expression of surface display SNAP. We can see that with increasing aTc concentration, there is a corresponding increase in fluorescent output (Figure 5A). Notably, fluorescent intensity peaks across all concentrations 3 hours after induction. Additionally, we see that there is no green fluorescence (Figure 5B) indicating that after there was no SNAP on the surface for the SNAP-Cell® 505-Star to hold onto. This could possibly be due to the bacteria becoming overgrown as the experiment continued, resulting in stress to the cells and a corresponding decrease in protein expression. In this first test we show that we have a circuit capable of single induction.

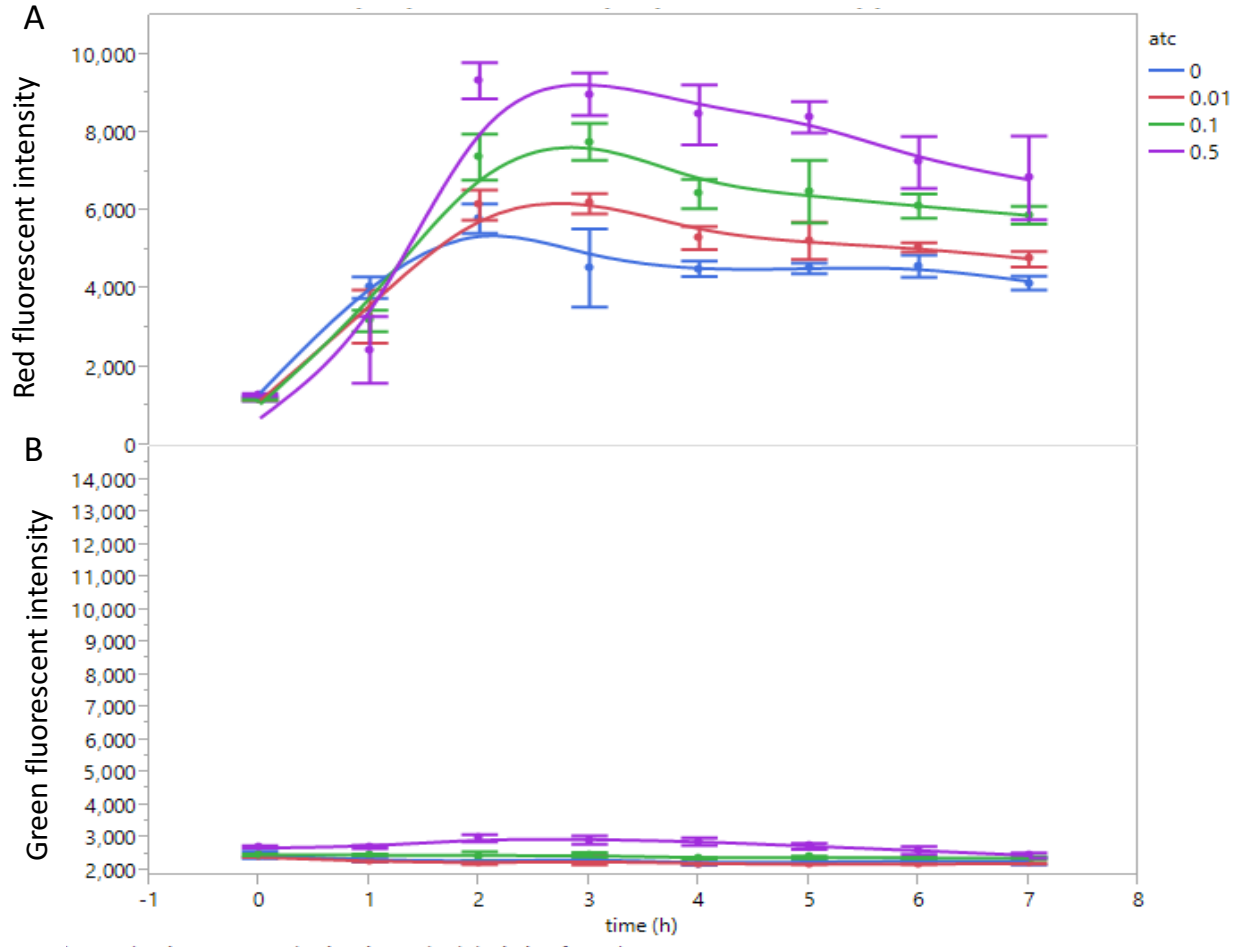

Figure 6: Dose response of orthogonal circuit with induction by aTc only resulting in cytosolic mCherry production. A) Red fluorescent intensity as a function of time and different concentrations of aTc. B) Lack of green fluorescent intensity indicating tight control of snap expression.

Next, to ensure that the lack of green fluorescence in Figure 6 was truly due to tight control and not due to an unfunctional genetic circuit, we tested induction of only the surface display SNAP circuit with arabinose (Figure 7). The results show a slight increase in fluorescent intensity of uninduced, labeled cells indicating a slight leak in expression. However, the fluorescent intensity never reaches the same peak as the induced cells. Additionally, similar to Figure 6, we note that peak fluorescent intensity occurs 3 hours after induction. Interestingly in this trial, the greatest fluorescence was noted in the 10^{-5} % arabinose despite a higher percentage being available to the

10^{-3} %. The difference in peaks is minimal but there is a noticeable drop after the peak in the 10^{-3} % arabinose. I hypothesize that the steep decline is due to the toxicity of arabinose to cells at a high concentration. The optimal concentration is therefore likely between 10^{-5} % and 10^{-3} %.

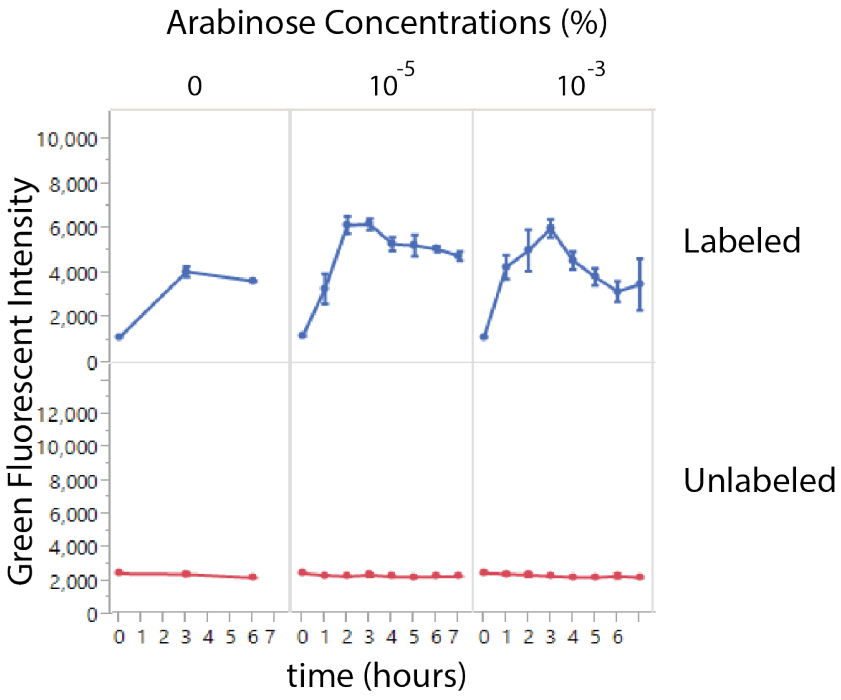

Figure 7: Induction of surface displayed SNAP with arabinose to show functionality. Varying concentrations of arabinose were used to test the induction potential of surface display SNAP. To confirm SNAP was on the surface of the cell, we labeled with SNAP-Cell® 505-Star (blue lines) and also measured unlabeled cells as a control (red lines).

Conclusion

Similar to microrobots, bacteria cells face spatial constraints when trying to design for multiple outputs and functions. Here, we have overcome the space limit in small bacteria cells by developing and well characterizing a system that uses the cell surface to spatially discretize synthetic protein output. Specific and direct applications of this technology include utilization of the cell's surface for controlled expression of proteins for selective small molecule capture, an avenue currently being pursued by our group. Thus, we are able to use engineered living cells as

surface-bound sensors and actuators, both capable of optically signaling the presence of selective molecules, and selectively binding to, and immobilizing, free-flowing substrates.

A similar solution could be considered for microrobotics, that is, to not focus on internalizing every component but to allow some to remain on the outside. While this is generally the location of most sensors, it is less feasible to think about keeping an electric circuit on the outside of a microrobot. If deployed in the environment or within the body, it would likely be quickly degraded by the various, harsh conditions often encountered in the outdoors, such as acidic rain or fluctuating temperatures, or within the body, such as the strong acidity of the stomach. Furthermore, if the components are biological, they are likely to trigger an immune response within our own system if they are readily available to immune cells. This reaction would either result in the destruction of the robot or a rising fever as our body tries to fight off foreign bodies. Ideally, we would be able to harness the best of the biological components within a non-living system for delivery.

Chapter 4: Modeling Information Exchange Between Artificial and Living Cells

Introduction

A microrobot's ability to sense its surroundings, process information, and act accordingly are crucial components to successfully navigate a diverse and changing environment. In this chapter we will explore modeling methods employed to probe interactions between an artificial cell, engineered living bacteria, and cell free synthetic circuits. As we discussed in the last chapter, putting components on the outer surface of microrobots may not be advisable due to extreme and changing environmental conditions. Yet even if the circuitry is encapsulated within a nonliving system we still do not fully understand how a microrobot will interact with its environment- including cells and molecules. With this model we hope to uncover the secret to multifunctional, cross system interaction.

In addition to whole cell synthetic biology, artificial cellular expression systems consist of minimal environments containing DNA templates, RNA polymerase, ribosomes, ATP, and other biological molecules relevant to a particular circuit [76]. Furthermore, all components can be spatially confined, such as on a microfluidic chip [77], or within a hydrophobic oil encapsulation [78]. Engineering artificial protocells has also provided significant insight into living systems [76, 77, 79]. Robust studies have been performed to understand the engineering concepts underlying the design of these systems [78].

Similar to the SNAP protein and BG modified substances, biotin and streptavidin (SA) are well known in biotechnology for having one of the strongest non-covalent bindings in nature [72]. Biotin is a water soluble, B-complex vitamin that is crucial to cellular metabolic processes, particularly gluconeogenesis and fatty acid metabolism [80]. Though humans obtain most of our necessary biotin from our diet, it has additionally been shown that our gut bacteria produce biotin

[81]. Clearly, biotin is an important biological molecule. Conveniently, biotin's affinity for SA allows for easy separation of biotin from solution. The biotin-SA binding is used in diverse applications from

Here, we extended and combined models of these well-described systems to explore ways in which living cells could be engineered to create artificial cells.

The following chapter shows results published in *Quantitative Biology* earlier this year [82].

Modeling Methods

Module One: The Engineered Cell

Module one consists of a population of *E. coli* cells engineered to contain gene networks capable of synthesizing biotin synthase, which in turn enables the cells to produce biotin. In previous publications, we detail how a continuous model, depicting the system's dynamic behavior, may be developed for complex regulatory gene networks [83, 84] as well as the biotin synthesizing processes [85]. This approach relies upon modeling four key subprocesses:

1) Inducer mass balance and binding kinetics
2) Transcription of mRNA from regulatory gene components
3) Translation of proteins, including reporters, repressors, and biotin synthase
4) Biotin metabolism

The first sub process is modeled by establishing three mass balance equations for a given inducer. These equations relate the concentrations of internal inducers, $[I_{int}]$, repressor proteins, [TP], and bound inducer-repressor complexes $[TP{:}I_{int}]$ within a cell (Equations 1-3). In addition to a simplified membrane flux term, these mass balances use first-order binding kinetics to relate the

relative concentrations of bound and unbound internal inducer and repressor protein complexes. A full derivation may be found in previously published literature by the group [84].

$$\frac{d([I_{int}])}{dt} = \mu([I_{ex}] - [I_{int}]) - K_a[I_{int}]\times[TP] + K_d[TP{:}\,I_{int}] - \delta_1\times[I_{int}] \quad (1)$$

$$\frac{d([TP])}{dt} = -K_a[I_{int}]\times[TP] + K_d[TP{:}\,I_{int}] + g[TP] \quad (2)$$

$$\frac{d([TP{:}I_{int}])}{dt} = K_a[I_{int}]\times[TP] - K_d[TP{:}\,I_{int}] - \delta_3\times[TP{:}\,I_{int}] \quad (3)$$

Equation 1 describes the time rate of change of the internal inducer concentration, I_{int}, as a function of four terms. The first term on the right hand side is a membrane transport term used to describe the mass flux of an inducer, such as IPTG, across the cell membrane. The second term is a kinetic association term that relates the internal concentration of an inducer, with the internal concentration of a transcription regulation protein, TP, and a kinetic association constant, K_a. The third term describes the disassociation of the repressor protein-inducer molecule complex, described by a disassociation constant, K_d, and the concentration of the bound complex, $TP{:}I_{int}$. Finally, the fourth term describes the decay of the internal inducer. It should be noted that for some inducers, such as lactose or arabinose, this fourth term is a function of natural cell metabolism.

Equation 2 describes the time rate of change of unbound transcription regulation protein available within the cell. The terms on the right hand side are analogous to those described in equation 1. However, there is an additional term describing the rate of regulation protein generated by the cell through the process of translation, g[TP]. Note that this translation process is described for a generic protein by equation 5, and that transcription factor proteins such as lacI or tetR, denoted as TP, are specific instance of a generic protein, denoted by P.

Finally, equation 3 describes the time rate of change of the bound inducer-transcription factor protein complex with terms analogous to those described in equation 2 and equation 3. Additionally, there is a decay term that is composed of a decay constant and the concentration of bound complex. It should be emphasized that this modeling approach was used for its simplicity and versatility to describe a wide array of inducer-repression complexes with the dynamics of the system emphasized.

The second sub-process, mRNA transcription, is modeled as a Hill-like function (equation 4) in order to capture the dynamics of the gene network without adding excess complexity. This approximation is justified by considering our system to contain a population of *E. coli* cells rather than relying on single-cell dynamics. The large population, coupled with a high copy count plasmid should mitigate significant statistical outliers. The equation relates the rate of mRNA synthesis with the concentration of the relevant reporter protein, the transcription leak, and the decay of mRNA.

$$\frac{d([mRNA])}{dt} = V_{1max}\left(\frac{1}{1+(\frac{[TP]}{K_b})^H}\right) + V_{1leak} - \delta_{mRNA}\times[mRNA] \quad (4)$$

Equation 4 describes the time rate of change of a generic mRNA concentration, mRNA, using three terms. The first term on the right hand side is a Hill-like function containing the maximum inducible rate of mRNA transcription, V_{1max}, the concentration of repressor transcription factor proteins, TP, a kinetic constant, K_b, and a Hill coefficient, H. The second term is a constant describing the amount of transcriptional leak within the cell, V_{1leak}, and the third term describes the decay of mRNA within the cell by relating a decay constant, $\delta_{mRNA,}$ and the mRNA concentration, mRNA.

Protein translation, the third sub process, is modeled by relating the rate of protein synthesis with the concentration of available mRNA, ribosome binding site strength (RBS), and a decay factor (equation 5). This equation is derived from Michaelis-Menten kinetics and is often used to model protein expression [86] when studying gene regulatory networks. Additionally, note that equation 5 is adapted and utilized within equation 2 as g[TP], the generation of a transcription factor protein. This inclusion allows us to account for transcription factor generation in the context of the binding kinetics described within equation 2. Additionally, the production of the protein biotin synthase can be recognized as a specific instance of a protein generated by the translation process described within equation 5.

$$\frac{d[P]}{dt} = V_{2max} \times RBS \times \frac{[mRNA]^m}{K_2{}^m + [mRNA]^m} - \delta_p \times [P] \quad (5)$$

With equation 5, we model the time rate of change for a generic protein, P, as a function of two terms. The first term describes the formation of the protein as the product of the maximum rate of translation, V_{2max}, a constant describing ribosome binding strength, and a Hill function relating the concentration of mRNA, with an activation coefficient, K_2, and a Hill coefficient, m. The second term describes the rate of decay for a specific protein, relating a decay constant, δ_p and the intercellular protein concentration for a generic protein.

Finally, the fourth sub-process describes the biotin formation by the cell. A simple model was developed for this process, inspired by Michaelis-Menten formalism, relating the concentration of available biotin synthase and DTB with the rate of biotin produced by the cell.

$$\frac{d[biotin]}{dt} = V_{3max} \times [bioB] \times \frac{[DTB]^q}{K_3{}^q + [DTB]^q} - \delta_{biotin} \times [biotin] \quad (6)$$

With equation 6, we model the time rate of change of biotin concentration, d[biotin]/dt, as the sum of a Hill function describing the rate of biotin synthesis and a decay term. The Hill function contains parameters describing the max rate of formation, V_{3max}, and an activation coefficient, K_3, and a Hill coefficient, q. Crucially, the rate of biotin formation is governed by the concentrations of both biotin synthase, bioB, and DTB. Parameters for this equation were bounded and fit using our previously published experimental data[85]. It should be noted that the rate of biotin decay is orders of magnitude slower than the rate of biotin formation, and as such the decay term can be largely ignored.

In our simulation, parameter values were taken from results previously published by other groups[87-91], as well as our own previously published experimental results[85]. As a characteristic example, the parameter values used for the inducer circuit shown in figure 6 were as follows: the IPTG relevant membrane permeability constant[89], $\mu = 5.0 \times 10^{-2}$ m^{-1}, the kinetic association constant[90], $K_a = 1.0 \times 10^3$, the kinetic disassociation constant, $K_d = 1.0 \times 10^{-2}$, and time-scale negligible decay constants[91], $\delta_1 = \delta_3 = 0$.

Equation 4-6 were fit using previously published data describing a planktonic culture of 3 mL of *E. coli* held at 37° C for 24 hours of growth[85]. Under these conditions, the transcription parameters are as follows: $V_{1max} = 3.0$ nM $\times$ m^{-1}, $V_{1leak} = 4.15$ nM $\times$ m^{-1}, $\delta_{mRNA} = 10.0$ m^{-1}, $K_b = 1.0 \times 10^2$ nM, and m = 2. Additionally, for the translation of biotin synthase, the parameters are: $V_{2max} = 6.2 \times 10^2$ nM $\times$ m^{-1}, $K_2 = 10.0$ nM, RBS = 1.0, m = 2, and $\delta_P = 1.0$ m^{-1}. Finally, for biotin synthesis, the parameters values were as follows: $V_{3max} = 6.2 \times 10^2$ ng $\times$ mL^{-1} $\times$ m^{-1}, $K_3 = 1.0 \times 10^2$ nM, q = 2, and $\delta_{biotin} \cong 0$.

Module Two: Streptavidin Functionalized Microbeads

Biotin-streptavidin interactions have been widely studied; here we were able to use a well-fit model from previously published results and apply it to our microbead system. Using this model (Equation 7) we can describe the competitive binding interaction between free biotin and biotinylated DNA for streptavidin sites. Modifying the concentration of biotinylated DNA introduced to the system allows us to shift the dynamic range of the curve higher or lower. A full derivation, as well as the experimental data to which the parameters were fit, was previously published by the authors [85].

$$\%SA_{DNA} = D + \frac{K_4 \times [Biotin_{DNA}] - D}{1 + K_4 \times [Biotin_{DNA}] + K_5 \times [Biotin_{Cells}]} \quad (7)$$

With equation 7, we model the percent of streptavidin sites bound to biotinylated DNA ($\%SA_{DNA}$) as a function of a background parameter, D, two association constants, K_4 and K_5, the concentration of biotinylated DNA, $Biotin_{DNA}$ and the concentration of cell-produced biotin. It should be noted that the cell produced biotin here, denoted as $Biotin_{cells}$, is the same as the biotin term from equation 6. The change in nomenclature was made to specify the source of biotin within equation 7.

For the simulation presented here, the following parameters were fit to previously published experimental data[85]: $D = 1.7 \times 10^{-4}$, $K_4 = 1.78 \times 10^{0}$ mL × ng^{-1}, $K_5 = 1.84 \times 10^{0}$ mL × ng^{-1}.

Module Three: Encapsulated Cell-Free Reactions

Cell-free reactions are frequently used in research, and a reliable model for the transcription and translation dynamics had been previously published in scientific literature [87]. This model relates the concentration of DNA, RNA, and proteins with the availability of transcriptional and translational resources within a cell-free encapsulation. This modeling approach allows one to model cell-free temporal dynamics under varying concentrations of DNA by simulating a set of five ordinary differential equations (equations 8-12).

$$\frac{d([GFP\_mRNA])}{dt} = V_6 \times \left(\frac{[TsR] \times [B\_DNA]}{K_6 + [B\_DNA]}\right) - \delta_{GFP\_mRNA} \times [GFP\_mRNA] \quad (8)$$

$$\frac{d([GFP])}{dt} = V_7 \times \left(\frac{[TlR] \times [GFP\_mRNA]}{K_7 + [GFP\_mRNA]}\right) - k_8 \times [GFP] \quad (9)$$

$$\frac{d([GFP^*])}{dt} = k_8 \times [GFP] \quad (10)$$

$$\frac{d([TsR])}{dt} = -\delta_{TsR} \times \left(\frac{[TsR] \times [B\_DNA]}{K_6 + [B\_DNA]}\right) \quad (11)$$

$$\frac{d([TlR])}{dt} = -\delta_{TlR} \times \left(\frac{[TlR]}{K_9 + [TlR]}\right) \quad (12)$$

With equations 8-12, [TsR] and [TlR] represent the concentration of available transcriptional and translational resources respectively. In addition, [GFP*] is the concentration of the fully formed GFP complex that may be monitored optically. Note that the concentrations of GFP encoding mRNA and biotinylated DNA, denoted as [GFP_mRNA] and [B_DNA] respectively, in equations 8-12 are in the cell-free reaction system and independent of the DNA and mRNA expressions from equations 6 and 7. Furthermore, the concentration of biotinylated DNA is a function of the fraction of streptavidin sites occupied by biotinylated GFP described by equation 7. The parameters V_6 and V_7 describe the maximum rate of transcription and translation,

respectively, whereas δ_{GFP_mRNA}, δ_{TsR}, and δ_{TlR} are decay constants for GFP encoding mRNA, transcriptional resources and translational resources, respectively. The parameter values for equations 8-12 were previously calculated and used in a model by Stogbauer et al.[87].

Taken together, the models for modules one through three allow us to simulate the cell-free response to inducer chemicals given to engineered cells. All simulations were coded in Python and numerically integrated using Runge-Kutta based methods within the NumPy library. Data visualization was prepared using the matplotlib library and figures were assembled using Inkscape open-source software. All simulations were performed on a 2012 MacBook Pro running macOS Sierra with a 2.9 GHz Intel Core i7 processor.

Results

As noted, there is a significant scientific incentive to create a system that allows engineered living cells to control and command the behavior of cell-free protocells. We designed such a system (Figure 8) by leveraging three previously demonstrated laboratory components: a biotin-synthesizing engineered living cell, a streptavidin-functionalized microparticle, and an encapsulated cell-free reaction. These three components, herein referred to as modules, can be strategically linked by the transport of two key analytes: biotin and biotinylated DNA. By developing a linked, reductionist model for these three components, we explored the dynamics of how engineered living cells could alter the response of protocell modules.

Module one (Figure 8A) consists of a population of engineered living cells. We previously demonstrated how *Escherichia coli* (*E. coli*) can be genetically engineered to synthesize elevated levels of biotin when provided with a biotin precursor, desthiobiotin (DTB), and exposed to an inducer molecule, such as Isopropyl β-D-1-thiogalactopyranoside (IPTG) [85]. Biotin is a

commonly used molecule in biotechnology due to the strength and versatility of the biotin-streptavidin binding event [88, 92]. Additionally, biotin may be readily used to functionalize DNA monomers by incorporating biotinylated primers in a PCR amplification of DNA segments, such as those encoding for the production of green fluorescent protein (GFP). Furthermore, streptavidin is frequently bound to substrates, such as polystyrene wells or nano- and micro-particles [93]. Module two (Figure 8B) exploits this technology by allowing cell-produced biotin and GFP-encoding, biotinylated DNA to compete for binding sites on streptavidin-functionalized microparticles.

Module three encapsulates these particles along with a cell-free TX-TL reaction to form a protocell (Figure 8C). Cell-free systems are widely used to explore biological phenomena such as gene network dynamics [94] and molecular assembly [95]. The intensity of a cell-free protein synthesis response is governed by the concentration of DNA available within the cell-free encapsulation. As such, in module three the intensity of a green fluorescent signal is proportional to the concentration of GFP-encoding, biotinylated DNA bound to the microparticles.

Taken together, these three modules provide a framework that enables programmable cells to control the response of cell-free protocells. In addition to engineering a strain of biotin producing cells, researchers have experimentally demonstrated a number of enabling technologies for all three modules. For instance, microfluidic channels (Figure 8D) may be used to contain, and provide nutrients to, populations of engineered cells [96]. These microfluidic chips allow ease of imaging [97] while keeping the contained cells in a prolonged exponential growth phase [96]. Additionally, streptavidin functionalized microparticles can bind to a biotinylated fluorophore eliciting a measurable fluorescent response (Figure 8E). Finally, GFP-encoding DNA may be

encapsulated within a droplet containing TX-TL cell-free extract [98] to elicit a strong fluorescent response (Figure 8F).

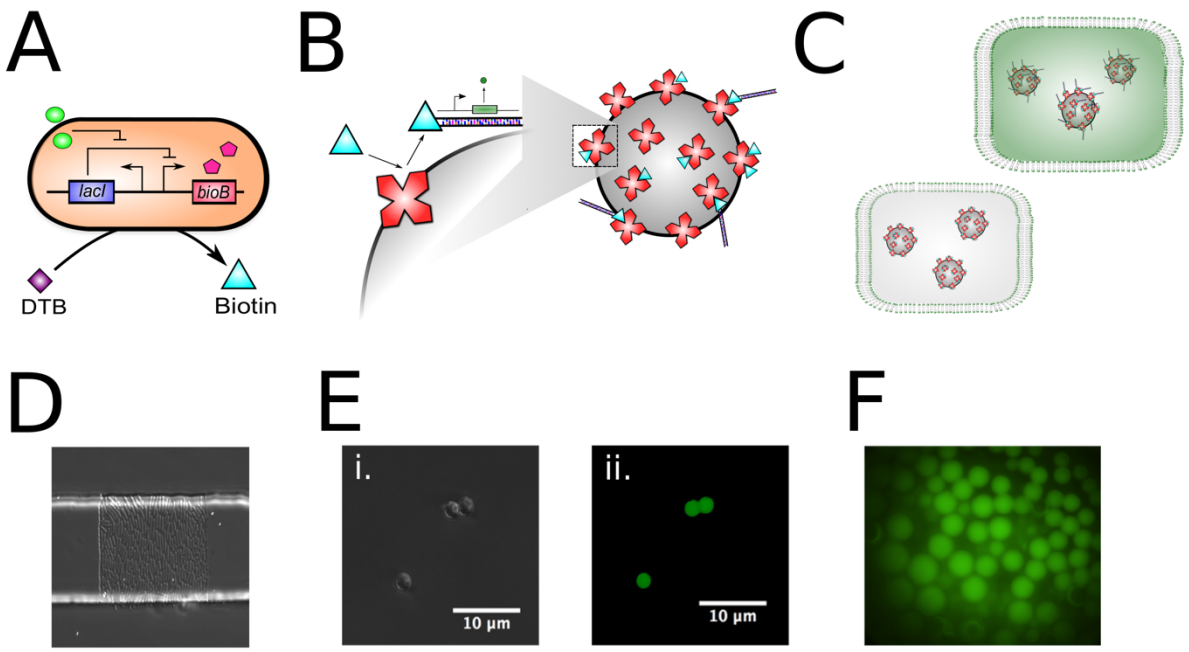

Figure 8: Linking engineered cells with cell-free systems. (A) Engineered cells synthesize biotin when exposed to a precursor molecule, desthiobiotin (DTB), and an inducer chemical such as Isopropyl β-D-1-thiogalactopyranoside (IPTG). (B) DNA encoding for GFP synthesis may be biotinylated. When in a solution together, biotin and biotinylated DNA compete for streptavidin binding sites. Streptavidin may be immobilized onto portable, micro- or nano- beads. (C) Beads are encapsulated with cell-free solution within a membrane to form a protocell. The protocell's transcriptional and translational behavior is governed by the concentration of DNA. (D) Genetically engineered *E. Coli* cells are trapped in a microfluidic channel. This allows engineered cells to stay in exponential phase growth, ensuring maximum metabolic efficacy. (E) Microbeads functionalized with streptavidin bind with biotinylated fluorophore causing a measurable fluorescent response. Here we depict a broadband image (E.i.) and a fluorescent image (E.ii.) captured using an epiflourescent microscope. (F) DNA encoding for GFP was encapsulated with TX-TL cell-free extract and buffer within oil-immersed droplets.

Additionally, all three modules may be modeled in a reductionist fashion from kinetic principles and simulated using established numerical methods. By providing a mathematical

underpinning for our system, these models enable predictive testing and insight, allowing us to better understand the governing dynamics of our system's cell-protocell interaction.

Module one leverages the tools of synthetic biology to genetically program the behavior of cells. Many well-established genetic motifs (Figure 9), inspired by electronic logic, have been synthesized and transformed into *E. coli* as well as other organisms. A simple gene regulatory network is the analogue inducer, or driver, circuit (Figure 9A.i.). Genes encoding for the repressor protein lacI are downstream from a constitutive promoter site [99]. In the absence of a chemical inducer, lacI binds to a P_{trc-2} promoter site, inhibiting the transcription of downstream sequences. However, when the inducer molecule IPTG is introduced to the cells, lacI disassociates from the DNA strand and binds with the available IPTG. This de-repression of the P_{trc-2} promoter site allows for transcription of downstream genes, such as *bioB,* a gene encoding for the production of the enzyme biotin synthase [100]. An electrical circuit analogy (Figure 9A.ii.) depicts the dynamics of this system, whereby additional IPTG causes an increase in biotin synthase production. This behavior may be simulated (Figure 9A.iii.) using commonly employed genetic models further described in the methods section [83, 86, 101].

Other well-established gene networks can be designed, modeled, and simulated in a similar manner. A simple modification to the inducer circuit is an inverter circuit (Figure 9B.i.) in which an inducing chemical, this time anyhydrotetracycline (ATc), attenuates the production of biotin synthase. This behavior is accomplished by placing the *lacI* gene downstream from a $P_{L,tetO-1}$ promoter site, and allowing the repressor protein, tetR, to be produced constitutively. In the absence of ATc, tetR represses the production of lacI, allowing for robust *bioB* transcription. However, when ATc is introduced to the system, it binds to the tetR repressor, in turn upregulating lacI synthesis. This has the effect of repressing the P_{trc-2} promoter site, decreasing *bioB*

transcription and translation. The electrical circuit analogy (Figure 2B.ii.) and simulated response profile (Figure 9B.iii.) confirm this behavior.

Similarly, an OR-gate, in which the presence of ATc or IPTG causes elevated levels of biotin synthase production, may be engineered (Figure 9C). This logic gate is accomplished by placing *bioB* downstream from both a P_{trc-2} and a $P_{L,tetO-1}$ promoter sites. Another commonly used genetic motif is the AND-gate (Figure 9D), in which only the presence of both ATc and IPTG will cause elevated levels of biotin synthase production [102]. This is accomplished by controlling the production of viral T7 polymerase, which in turn binds to a T7 promoter site driving *bioB*. With only IPTG present, this system creates short non-coding hairpin RNA sequences. When only ATc is introduced, the AND-gate transcribes an RNA encoding for T7 that has been compromised with internal stop-codons. However, when both ATc and IPTG are introduced to the cell, the hairpin RNA sequences bind to the superfluous stop codons on the T7 polymerase RNA sequence. This allows for effective translation of the T7 polymerase, which in turn activates biotin synthase production. Finally, we can model a toggle-switch (Figure 9E), in which sustained periods of activation or repression may be triggered by a transient pulse of either ATc or IPTG [103, 104]. This behavior is accomplished by designing the *lacI* and *tetR* genes to be mutually repressed. Simulated behaviors for the OR-gate, AND-gate, and toggle switch (Figures 9C, 9D, and 9E) provide us with predictable insight into the dynamic behavior of these gene regulatory networks.

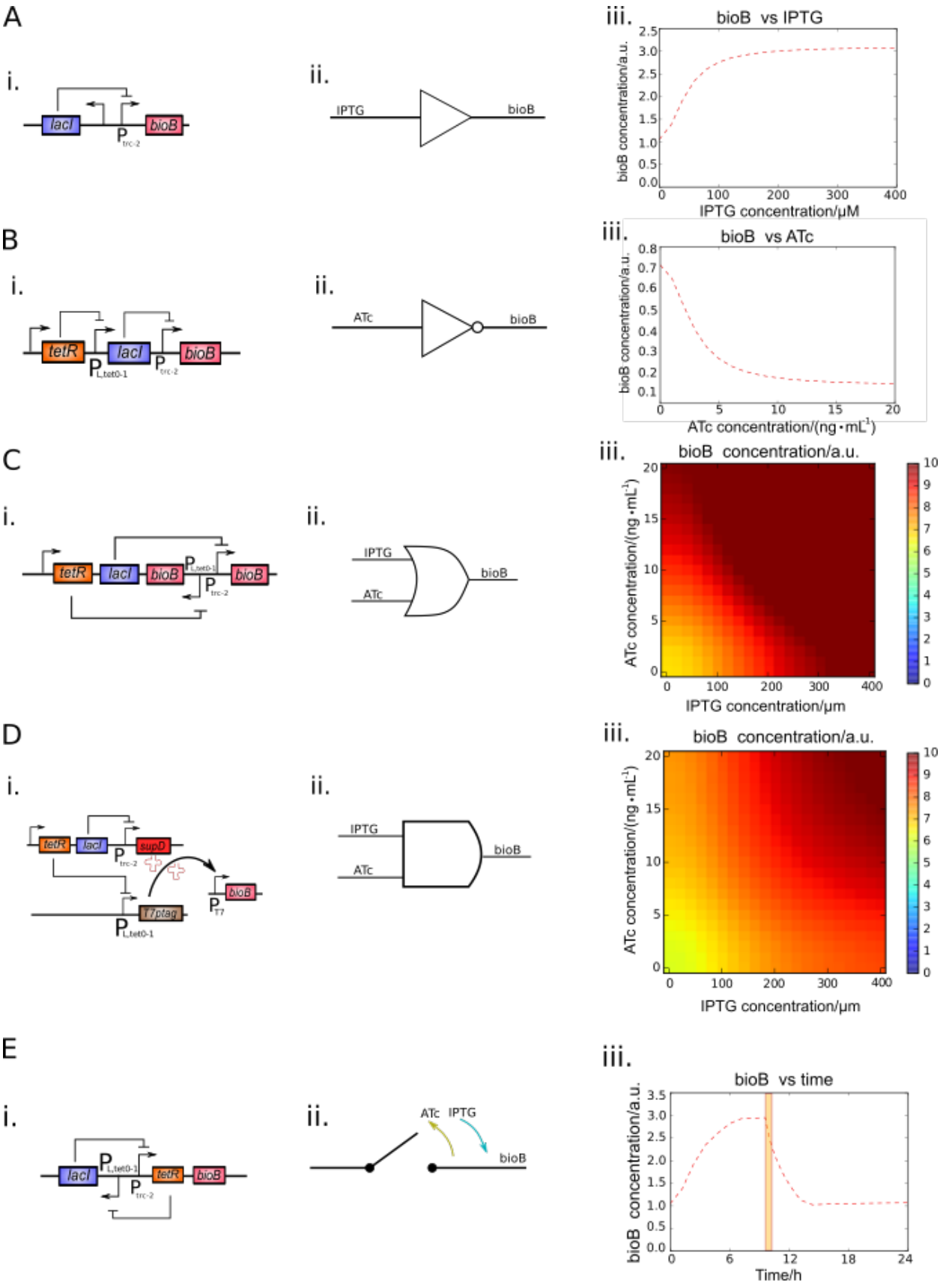
A
i.
lacI
bioB
ii.
IPTG
bioB
iii.
bioB vs IPTG
bioB concentration/a.u.
IPTG concentration/μM
B
i.
tetR
lacI
bioB
ii.
ATc
bioB
iii.
bioB vs ATc
bioB concentration/a.u.
ATc concentration/(ng·mL-1)
C
i.
tetR
lacI
bioB
bioB
ii.
IPTG
ATc
bioB
iii.
bioB concentration/a.u.
ATc concentration/(ng·mL-1)
IPTG concentration/μm
D
i.
tetR
lacI
supD
bioB
T7ptag
ii.
IPTG
ATc
bioB
iii.
bioB concentration/a.u.
ATc concentration/(ng·mL-1)
IPTG concentration/μm
E
i.
lacI
tetR
bioB
ii.
ATc
IPTG
bioB
iii.
bioB vs time
bioB concentration/a.u.
Time/h

Figure 9: Programming engineered cells. Synthetic gene regulatory networks are used to control the behavior of engineered cells. (A) The inducer gene regulatory network (A. i.) consists of a lacI repressed promoter site driving the transcription of bioB, an enzyme necessary for biotin synthesis. Then when introduced, IPTG binds to lacI, inhibiting lacI's ability to repress the promoter site. This induces the synthesis of bioB. An electrical logic abstraction is shown (A.ii.) to illustrate this system. Existing predictive, continuous models allow us to simulate this circuit's behavior (A.iii.). Similar representations are shown for a genetic inverter (B), a genetic OR-gate (C), a genetic AND-gate (D), and a genetic toggle switch (E).

However, biotin synthesis is a function of both *bioB* regulation and the cell's access to available DTB. Previously, we developed equations for a response profile by fitting basic enzyme kinetic equations with experimental results [85, 105]. Taking the resulting equations, and coupling them with the biotin synthase response profiles developed in Figure 9, we can model and simulate biotin synthesis as a function of inducer molecules and available DTB. After simulating an inverter circuit, the biotin response profile (Figure 10) depicts a decrease of biotin production as more ATc is added to the system while showing that an increase in DTB causes an increase in biotin production. This is the expected response; the inverter circuit attenuates *bioB* transcription, and thereby biotin formation, as more ATc is introduced to the cells. Similar response profiles may be simulated for all of the gene networks presented in Figure 9, allowing us to rationally design gene networks for a predictable biotin response.

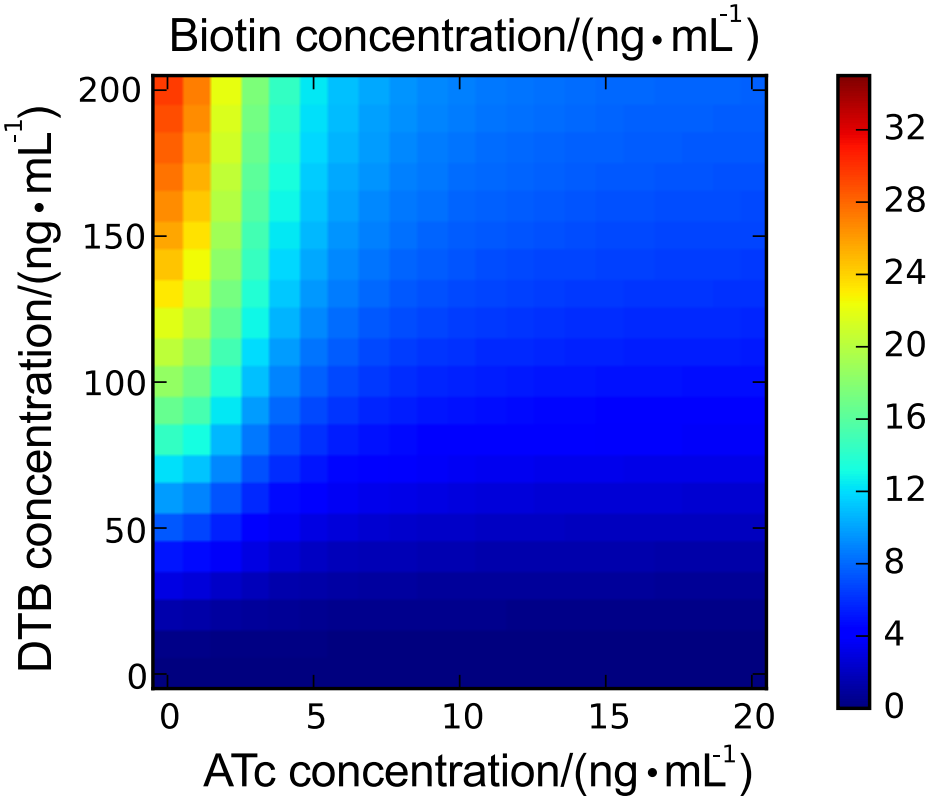

Figure 10: **Controllable biotin synthesis from engineered cells**. By genetically engineering cells to contain a gene regulatory network encoding for bioB synthesis, we can simulate the resulting biotin produced as a function of DTB and an inducer chemical, anhydrotetracycline (ATc). Here we simulate a cell containing an inverter (Fig. 2B) gene network. The cell's ability to synthesize biotin was modeled using first principle kinetics coupled fit to experimental findings previously reported. Biotin synthesis increases as DTB increases, but decreases as ATc increases. This aligns with the inverter's programmed behavior.

Module two exploits the versatility of the biotin-streptavidin bond. By establishing a competitive binding interaction between biotin produced by the engineered cells, and biotinylated DNA, we can predictably model the percent of streptavidin sites occupied by biotinylated DNA for an experimentally relevant range of biotin concentrations. This model (Figure 11A) employs a four-parameter logistic response profile, fit with previously published constants and experimental data [85, 106]. Furthermore, it allows us to explore how altering the concentration of biotinylated DNA (orange, yellow, blue, black) can affect the response of the initial (green) curve.

Coupling this competitive binding response function with information about the streptavidin-functionalized microparticles allows us to calculate the concentration of biotinylated DNA bound to the particles. A two-dimensional response profile (Figure 11B) may be developed relating the concentration of DNA per-weight of particle to the concentration of biotin and the radius of the particles. Note that smaller particles and lower concentration of biotin cause a larger concentration of bound, biotinylated DNA. This profile enables effective experimental parameter tuning by predictively altering the size of particles and dilution of biotin.

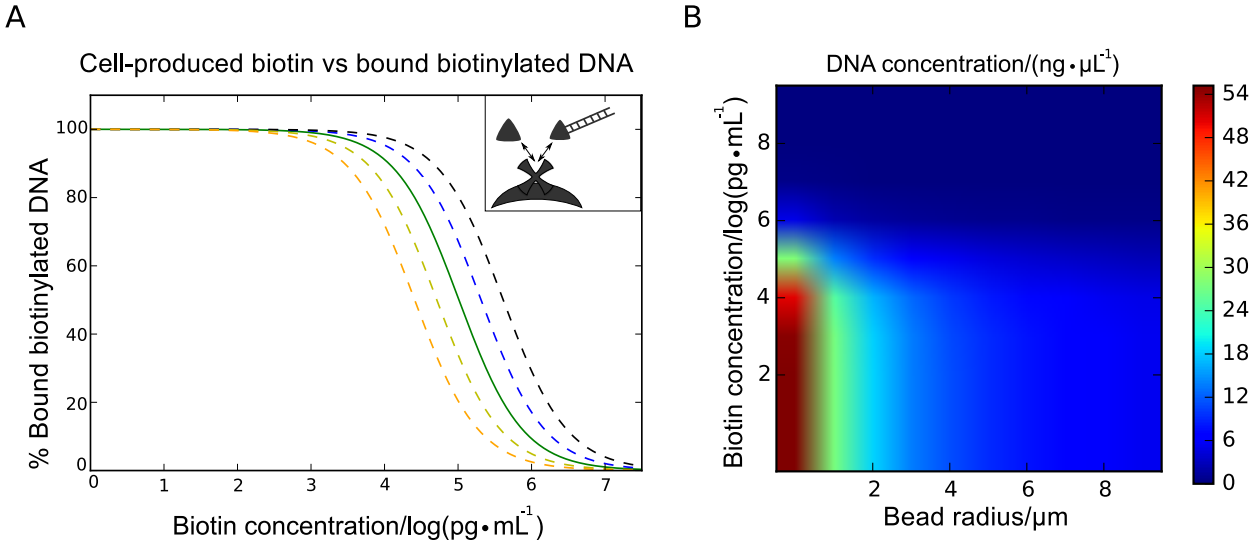

Figure 11: **Functionalized microparticles interact with cell-produced biotin**. Cell-produced biotin and biotinylated DNA compete for streptavidin binding sites. Streptavidin is immobilized onto a portable, microbead. (A) The competitive binding dynamics are modeled and tuned with previous experimental results (green). Shifts in the dynamic range occur by altering the concentration of biotinylated DNA within the system (yellow, orange, blue, black). (B) Total bead-bound DNA concentration per weight of beads may be calculated as a function of cell-produced biotin and the radius of the bead selected.

Module three is an encapsulation composed of DNA (bound to microparticles) and cell-free extract. This module allows us to monitor the behavior of a cell-free system by examining an encapsulated droplet and analyzing the fluorescent response [107]. By modifying the concentration

of DNA encoding for GFP within a cell-free system, previous studies have developed a reliable framework for modeling cell-free response as a function of DNA concentration [87]. Here, we simulate the temporal response for three concentrations of DNA (Figure 12A) and then plot the maximum GFP expression (Figure 12B) as a function of initial DNA concentration. We find that there is an asymptotically stable response profile relating the DNA concentration to the fluorescent intensity. This curve suggests that reactions employing low concentrations (0.0-20.0 ng/uL) of DNA will result in larger fluorescent intensity charges, a favorable experimental condition.

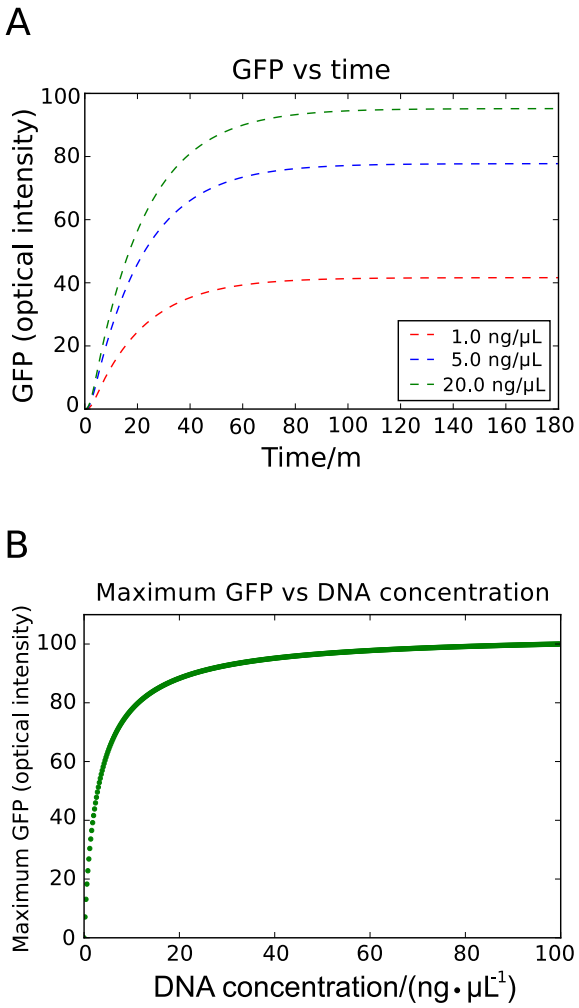

Figure 12: **Optical response of a cell-free system**. (A) The transcriptional and translational temporal dynamics of a cell-free systems may be modeled as a set of five ordinary differential equations, and simulated. (B) The maximum/steady-state levels of GFP produced by a cell-free system may be plotted as a function of the DNA concentration. This plot reveals how by

attenuating the concentration of DNA introduced to a cell-free system, one may limit the intensity of the fluorescent response.

The models for all three modules may be linked by strategic chemical transport. The biotin produced by module one directly affects the competitive binding in module two which in turn directly affects the concentration of DNA encapsulated within the cell-free system. By specifying experimental conditions, such as DTB concentration and particle sphere radius, the linked modules model allow us to simulate cell-free fluorescent response as a function of the inducer concentration exposed to the engineered cells (Figure 13).

First, we simulate a biotin response profile for a population of engineered cells (Figure 13A). We chose to simulate the inducer/driver circuit for illustrative purposes. By specifying a concentration of DTB, we can plot the concentration of biotin produced as a function of IPTG. Passing this biotin through module two, we can calculate the percent of particle-bound biotinylated DNA (Figure 13C) as a function of IPTG. Upon selecting a particle radius, we can calculate the concentration of DNA bound to the particles, which may be used to simulate a cell-free response (Figure 13D). By indexing the simulated DNA concentrations with the IPTG concentrations, we can plot a function relating the concentration of IPTG given to the engineered cells with the GFP production within the cell-free system (Figure 13E). In such a manner, we can simulate and predict how engineered cells can control the behavior of cell-free encapsulations and protocells.

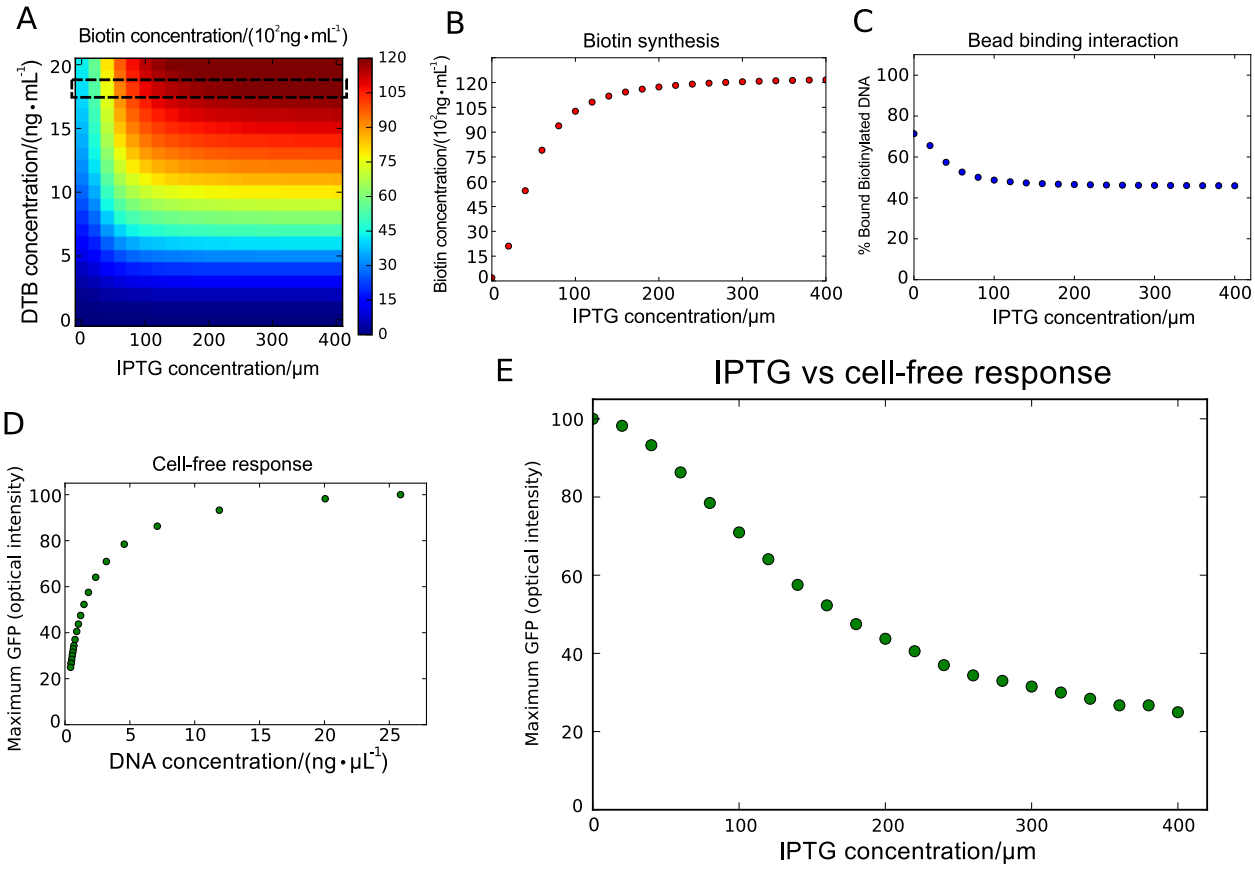

Figure 13: **Engineered cells control the dynamics of cell-free protocells.** (A) Biotin synthesis response profiles may be developed for a line of cells engineered to contain an inducer circuit. (B) By holding the levels of precursor DTB constant, biotin synthesis may be calculated as a function of the inducer molecule, IPTG. (C) By using the cell-produced biotin profile, and the curves developed for the streptavidin binding dynamics, we can model the percent of bound, biotinylated DNA as a function of the IPTG introduced to the cells. (D) By selecting for a constant bead size, we can model how the concentration of biotinylated DNA attached to the beads would affect a cell-free response profile. (E) By mapping the response profile from (C) through the cell-free dynamics response in (D), we can model how IPTG concentrations exposed to engineered cells would affect the fluorescent response of a cell-free system.

Discussion and Conclusion

As previously discussed, the key hypothesis we explored is the possibility that living cells can be engineered to direct the assembly of genetic components required for protocells, potentially revealing a possible complex biological behavior motif. Our work here explores one component of this, the assembly of DNA circuitry on a programmable material scaffold and opens the door to

the possibility that cells could assemble complex systems from materials scavenged from their environment. Moreover, microbes have frequent access to these building blocks of life as cell death ends in lysis, and the result is a microbial environment awash in functional macromolecules.

In the work here, we showed how a single population and cell strain could be developed to control assembly. However, there is also the promising potential to use an engineered consortium [108-110] for similar molecular assembly. These complementary synthetic systems have already been introduced. As a first step, programmable material surfaces would be engineered that serve to anchor individual components of engineered genetic circuits. Living cells would then be engineered to program the self-assembly of circuit components on these material surfaces similar to the ways that have been demonstrated. The assembled genetic circuits will then be assayed using a cell-free, gene expression system. As a second step, given that we encoded most of the information exchange between modules using the transport of biological molecules, a microfluidic system enabling the rapid, controlled assembly of biological materials within liposomes could be developed as a critical enabling technology. Both the engineered living cells and the microfluidic assembly system could be combined in the development of a unique ecological consortium consisting of living cells and non-living, cell-inspired material systems. In these experiments, a mixture of living cells and the artificial cells they assemble would be engineered to be co-dependent members of an engineered consortium [111]. The living components of these systems will only propagate if they continue to participate in the assembly of the non-living artificial cells.

By creating these types of engineered microbial and artificial cell consortia, we believe that a range of problems could be explored where diverse synthetic biological systems would be useful, ranging from drug delivery to materials science.

Chapter 5: Modulation of synthetic circuit expression in a cell free system with a microparticle scaffold

Introduction

As stated in the previous chapter, there are numerous advantages to linking biological and nonliving components through the use of a functionalized microparticle scaffold. After successfully modeling the competitive binding interaction between biotin and biotinylated DNA for the SA binding sites on a functionalized microparticle, we now seek to test whether these models hold for experimental observation. Though we modeled complex architecture and synthetic circuits, we will focus on a very simple structure in this section, a biotinylated DNA strand encoding GFP synthesis. This construct is chosen as the simplest way to test our hypothesis: can we experimentally control protein expression using a microparticle scaffold and the biotin-SA interaction? Here we successfully answer this question and develop an enabling technology capable of modulating a measurable output (GFP expression) based on environmental factors.

Materials and Methods

Obtaining biotinylated DNA

The biotinylated DNA that will be competing with free biotin for SA sites on the microparticle encodes a synthetic circuit with the promoter $P_{L,tetO-1}$ driving GFP. This DNA is obtained by performing a PCR with biotinylated primers on the plasmid $pZE_{2,1\text{-}GFP\text{-}\Delta EcoRI}$. The forward primer is biotinylated and binds 100 base pairs upstream of the promoter ensuring any upstream promoter interaction is intact. The reverse primer is not biotinylated and binds to the terminator. For the control run, a non-biotinylated forward primer is used. After PCR, the product is loaded into a gel made of TAE with 1% agarose. Electrophoresis was run at 110 mV and 220 A for 45 minutes and

the product was then extracted using a gel extraction kit. The result is a linear, double stranded DNA fragment (1112 bp in length) which serves as the template in the cell free reactions. The primers are listed below in Table 1, reaction composition is given in Table 2, and thermal cycler conditions are shown in Table 3, and a schematic is shown in Figure 14.

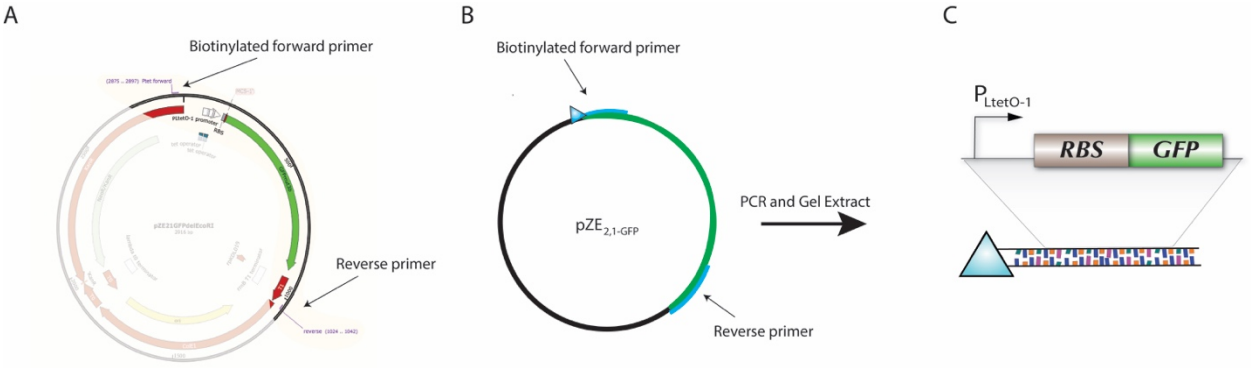

Figure 14: Obtaining biotinylated DNA by PCR with biotinylated primers. Method used to obtain biotinylated DNA samples using PCR. A) Plasmid map from SnapGene showing placement of primers used, B) representative schematic of part A showing the biotinylated forward primer and the non-biotinylated reverse primer. C) Final product after PCR, electrophoresis, and gel extraction results in a linear, biotinylated, double stranded DNA template encoding GFP.

Table 1: Primer Sequences used in PCR of GFP from $pZE_{2,1\text{-}GFP}$

Primer Name	Sequence
TetGFP_f	GGCTTCCCAACCTTACCAGAGGG
GFP_r	CGCCTAGGTCTAGGGCGGC

Table 2: Reaction Composition for PCR

Reaction Composition	
Template DNA	Vt µL
Primer mix	1.25 µL
10x buffer	2.5 µL
dNTPs	0.5 µL
Taq	0.25 µL

H20	(20.5-Vt) µL
Total Volume	25 µL

Table 3: Thermal Cycler Conditions for Touchdown PCR

Thermal Cycler Conditions		
Initial Denaturation	3 min	95 °C
Touchdown Cycles		
Denature	20 sec	95 °C
Anneal	20 sec	70 °C
	-1 per cycle	
Extend	1 min/kb	72 °C
15 Cycles		
Constant Cycles		
Denature	20 sec	95 °C
Anneal	20 sec	55 °C
Extend	1 min/kb	72 °C
20 Cycles		
Final extension	5 min	72 °C
Hold	indef	4 °C

Binding biotinylated DNA to SA functionalized microparticles

Biotinylated DNA was created using the protocol shown above. Varied concentrations of biotinylated DNA, and free biotin, are mixed with SA coated, 2.29 um diameter, red fluorescent, paramagnetic microparticles (Spherotech ®, FSVM-2058-2). Generally, 0.5 µg of biotinylated DNA was mixed with 20 µL of 0.1% w/v microparticles and the final volume was brought to 50 µL with filtered PBS. If any free biotin is needed for the experiment, it is added to the biotinylated DNA mixture before the addition of the microparticles and then the final volume is brought up to the desired amount with PBS. The mixture is then allowed to react with slow vortexing for 2 hours at room temperature. The solution is then centrifuged for 1 minute at 5000 rpm to pellet the microparticles and the tubes are placed on a magnetic rack to further separate out the

microparticles. The supernatant is removed and the microparticles are re-suspended in 100 μL of PBS. This procedure is repeated 5 times with no resuspension on the last rinse cycle.

Creating the cell free reaction components

The TX-TL cell-free expression protocol from the Noireaux lab [55] was used to make the components of the cell-free reaction. First, crude cell extract was made using frozen stocks of Rosetta™ (DE3) *E. coli* BL21 cells, genotype *F- ompT hsdSB(rB- mB-) gal dcm (DE3) pLysSRARE (CamR)* grown in 2xYT+P and chloramphenicol (Cm) media. Cultures were grown for 8 hours at 37°C with agitation at 220 rpm. The cells were then by subcultured and further incubated under the same conditions for an additional 4 hours (OD_{600} = 1.5-2.0). The cells were then pelleted through centrifugation and washed using S30A buffer. After centrifuging, the pellet was weighed. S30A buffer and 0.1 mm glass beads were then mixed with the pellet through vigorous vortexing. The bead-cell mixture was aliquoted into bead beating tubes and cells were lysed by bead beating each tube twice at 46 rpm for 30 seconds. To remove the beads, micro-chromatography columns were pressed to the ends of open tubes after beating and were centrifuged. Of the eluted sample, the supernatant was collected and incubated for 80 min at 37°C with 220 rpm agitation to further digest nucleic acids with endogenous exonucleases. The samples were spun down again and the supernatant was collected and dialyzed using 10k MWCO dialysis cassettes submerged in S30B buffer with stirring for 3 hours at 4°C. The processed extract was spun down one last time and the supernatant was divided into 30 μL aliquots, flash-frozen, and stored at -80°C. Protein concentration (30 mg/ml) of the extract was measured using a Bradford assay.

Amino acid and energy solutions were combined into buffer solutions and calibrated according to previously published protocols [112]. The plasmid $pZE_{2,1\text{-}GFP}$ ($P_{L,tetO\text{-}1}$ driving GFP expression) was used to visualize protein production within the cell-free system. Optimal concentrations of Mg-glutamate, K-glutamate, and dithiothreitol (DTT) were determined experimentally, and found to be 6 mM, 140 mM, and 1 mM, respectively (Figure 15). In addition, each experimental reaction also consisted of 1.5 mM amino acids, 1X energy solution, 2% PEG-8000, 33% extract, and DNA. The concentration of DNA may be adjusted by calculating the molar concentration of the stock and varying the ratio of DI water to DNA during reaction construction.

Running a cell-free reaction

The cell free expression system used consists of a three tube reaction: the cell extract, the buffer, and the DNA. The buffer and cell extract are first mixed in a 5:4 ratio. The DNA is then added in the desired concentrations keeping the total reaction volume of a single tube below 15 μL. If microparticle bound DNA is used as the source, the microparticles are suspended directly in the buffer/cell extract solution following the last rinse cycle. PBS is added as needed to bring the final reaction volume up to 10 μL. The tubes containing the reaction mixture are then placed into a 29 °C environment (thermal cycler or incubator) and allowed to react for 10-12 hours. If imaging cannot be completed immediately following this time period, the reaction is placed into a 4 °C environment to stop the reaction.

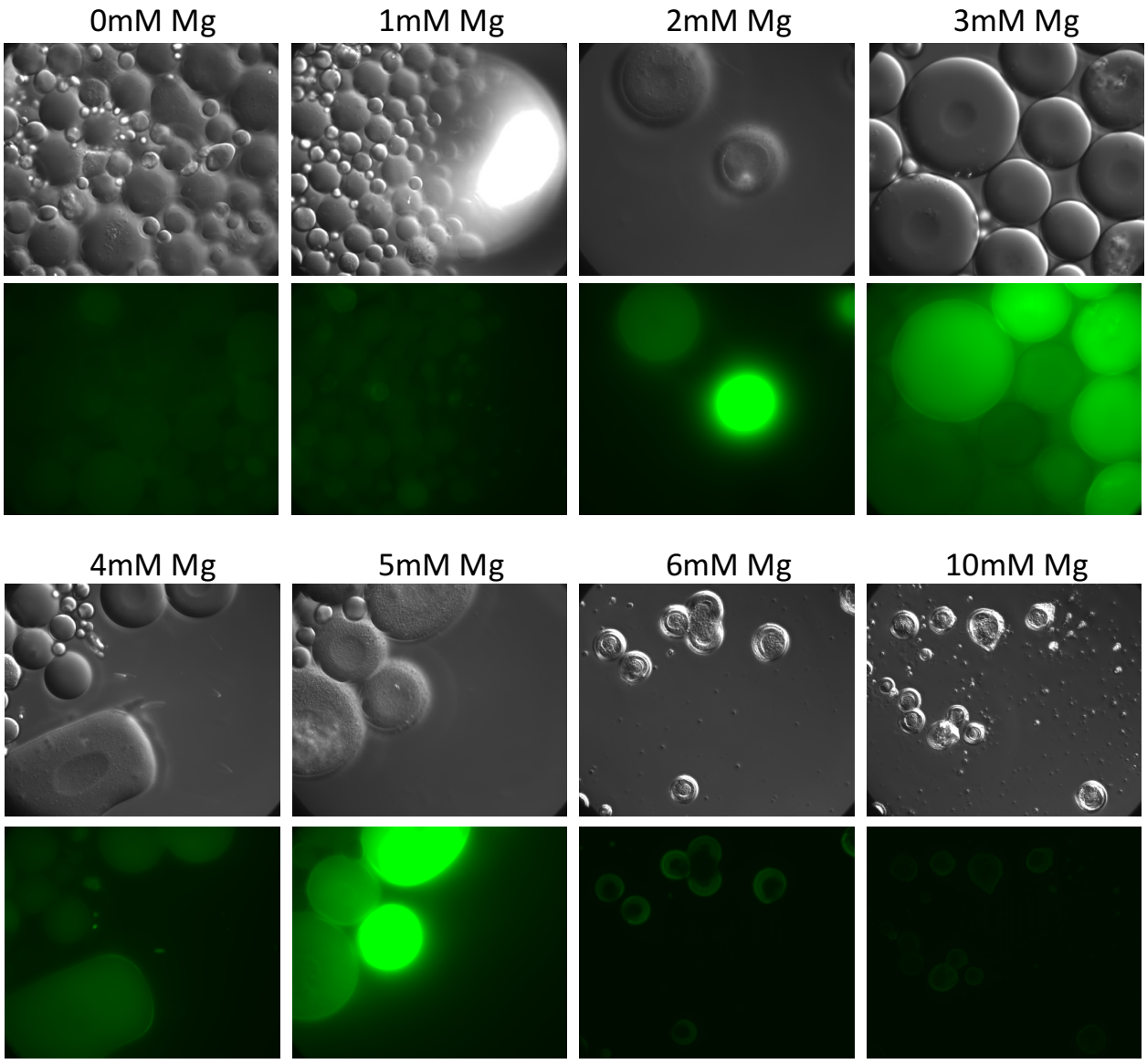

Figure 15: Optimization of salt concentrations for cell free solutions. The results for the optimization of Mg-glutamate in the buffer for cell free reactions is shown here for concentratiosn ranging from 0-10 mM. A final concentration of 5 mM was chosen after measuring the mean FITC and the procedure was repeated for K-glutamate and DTT to optimize protein yield in the cell free expression system.

Microfluidic Master Mold Fabrication

All imaging was completed using a microfluidic chamber to house the reaction (described in the next section). The microfluidic master molds used in this procedure were fabricated in the Virginia Tech Micro & Nano Fabrication Laboratory (MICRON) (Figure 16). Photomasks were drawn in

AutoCAD (San Rafael, CA), printed onto transparency film by CAD/Art Services, Inc. (Output City, Poway, CA), and mounted onto glass plates (McMaster-Carr, Los Angeles, CA). The first layer of the master mold was created by spin coating a layer of SU-8 2100 negative photoresist (MicroChem Corp., Newton, MA) onto a clean silicon wafer to a height of 100 μm using a WS-650-8B programmable spinner (Laurell Technologies Corp., PA). Then the photoresist was exposed to ultraviolet light (UV) using a MA/BA6 UV contact mask aligner (MicroTec, Garching, Germany). After UV exposure, the wafer was rinsed using a developer (MicroChem Corp., Newton, MA) to remove residual, unexposed photoresist. The chamber dimensions are 4 mm x 2 mm with a height of 100 microns.

Replica molds were next created from the master molds using PDMS/Sylgard 184 (Dow Corning, Midland, MI) which was mixed at a 10:1 ratio with an elastomer base curing agent. This mix was poured on top of the wafer, and allowed to degas in a vacuum desiccator for 1 hour. The mold was then cured in an oven at 90 °C for 30 minutes. The PDMS chips were then removed from the oven, and holes were punched into the central circles at either end of the chip to allow proper for proper flow. The PDMS chips were then strongly bound to clean coverslips (Thermo Fisher Scientific, Waltham, MA) by exposing both surfaces to oxygen plasma for 1 minute in the PDC-32G plasma cleaner (Harrick Scientific, Ithaca, NY) and placing the exposed surfaces together. The bound chip and coverslip was allowed to cure for 6 hours at 90 °C before use.

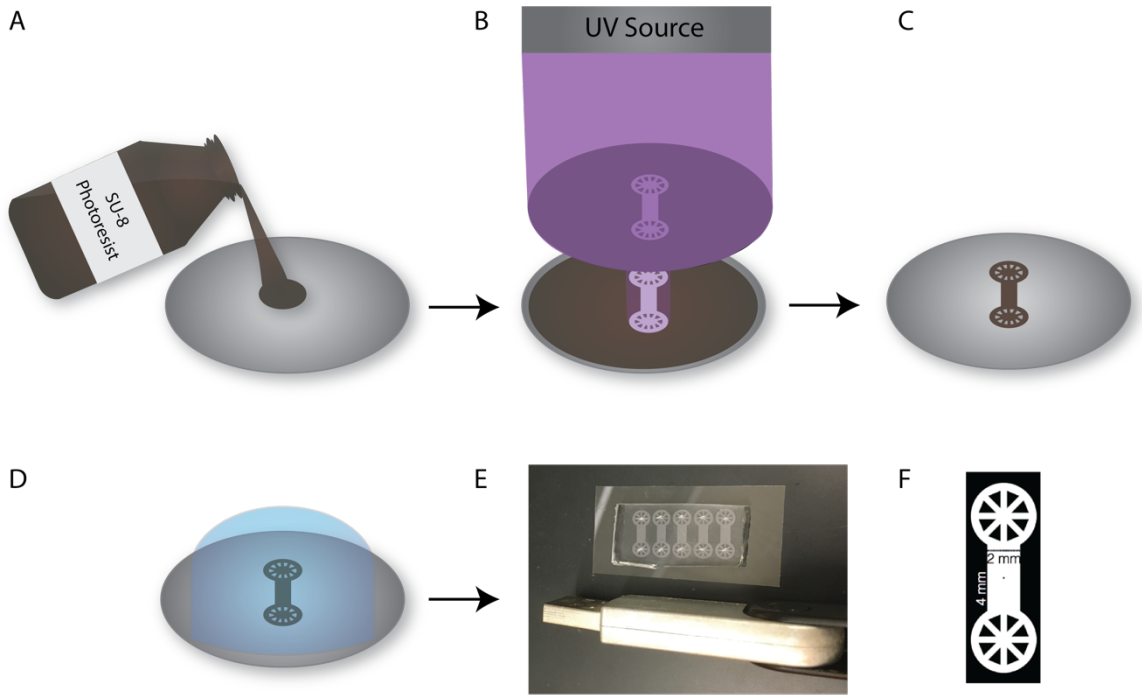

Figure 16: Microfluidic chip fabrication. A) Pouring of SU-8 2100 photoresist onto a silicon wafer and spinning the photoresist using a spin-coater to achieve a uniform height. B) UV exposure of the silicon wafer with photoresist using a custom design pattern. C) After developing the exposed substrate on the wafer we are left with a channel of our choice. D) PDMS can then be poured onto the patterned wafer surface, in this case with channels achieving a height of 100 um. E) The finalized microfluidic chips used for imaging in this section with a flash drive for size reference. F) The channel dimensions of the design used to fabricate the microfluidic chips, showing a 2 mm x 4 mm main channel in which imaging was conducted.

Imaging and quantification procedure

After completion of the cell free reaction, the tubes are centrifuged for one minute at 5000 rpm to pellet the microparticles. Next, 5 µL of cell free mixture (without microparticles) is pipetted into 10 µL of oil HFE 7500 (3M™ Novec™) with 1.8 % of the surfactant KRYTOK® 157 HFE (DuPont™). This oil encapsulation step provides spherical "bubbles" of cell free reaction suspended in oil thereby allowing for easier image quantification and analysis. The mixture is then vortexed and 2 µL is pipetted off the top layer injected into the microfluidic chip (Figure 17A). Imaging is then performed using an inverted epifluorescent microscope (Ti-E, Nikon Instruments

Inc.), 40x oil objective with 100 ms FITC exposure, 100 ms DIC exposure, and 200 ms TRITC exposure times.

Analysis is performed on the resulting image to quantify the fluorescence present. Circular regions of interest (ROIs) of equal size are drawn onto three different bubbles in the image. A fourth ROI is placed in a background area where no cell free bubbles are located (Figure 17B). The mean FITC is then quantified using the NIS Elements Software package. The first three ROIs are background subtracted and then averaged to obtain the given fluorescent intensity for that image. The process is repeated for all images.

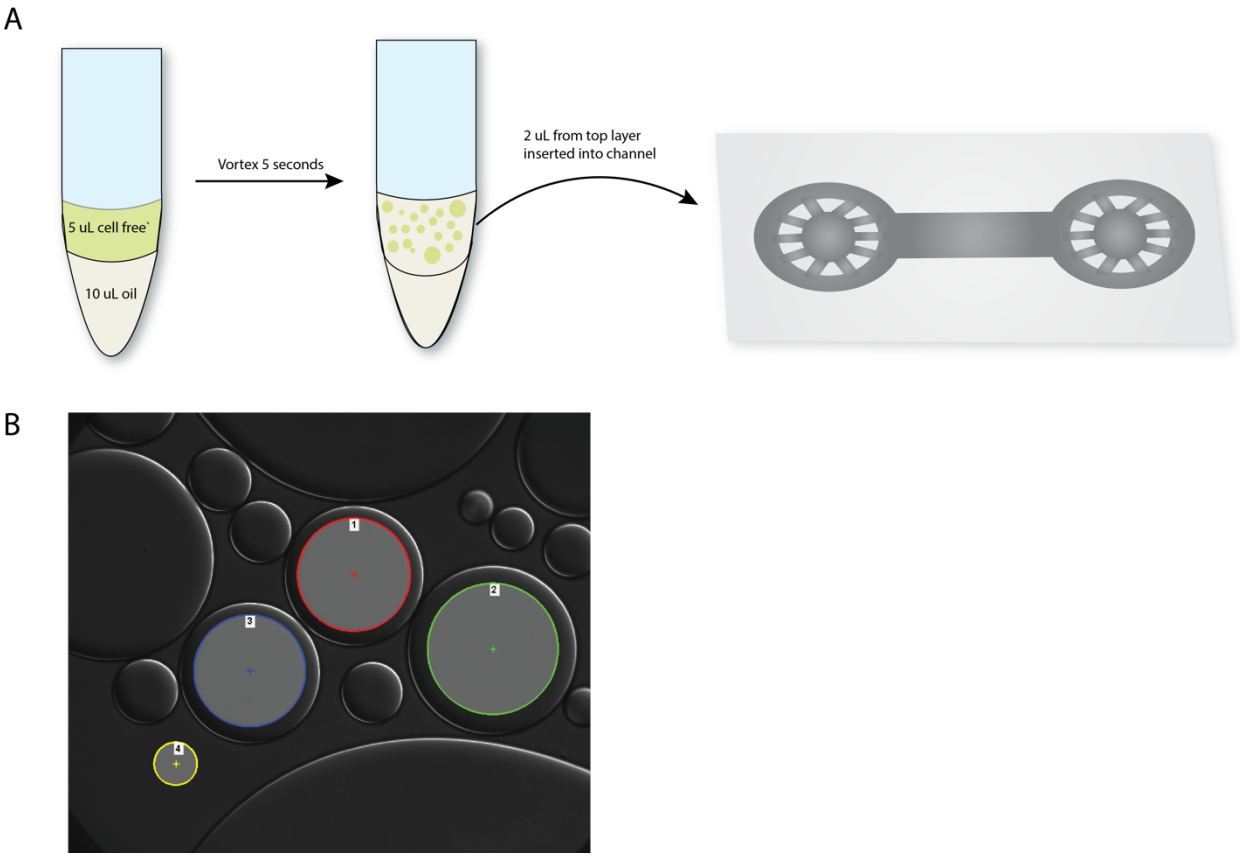

Figure 17: Imaging and quantification procedure. A) Encapsulation of cell free reaction within an oil solution and insertion into a microfluidic chamber for imaging. B) Sample ROI placement

for optimal image analysis using the NIS Elements Software package. Mean FITC was taken for each ROI and averaged before subtracting the background value.

Results

To start, it was imperative to confirm that the biotinylated primers were producing the desired product. After completion of a PCR following the protocol shown in Table 3, the product was measured using gel electrophoresis in a 1% agarose gel. When viewed on a UV imaging doc after 45 minutes of electrophoresis, the product is seen to be slightly larger than 1000 base pairs (Figure 18) which aligns with the size of 1112 base pairs that was designed for.

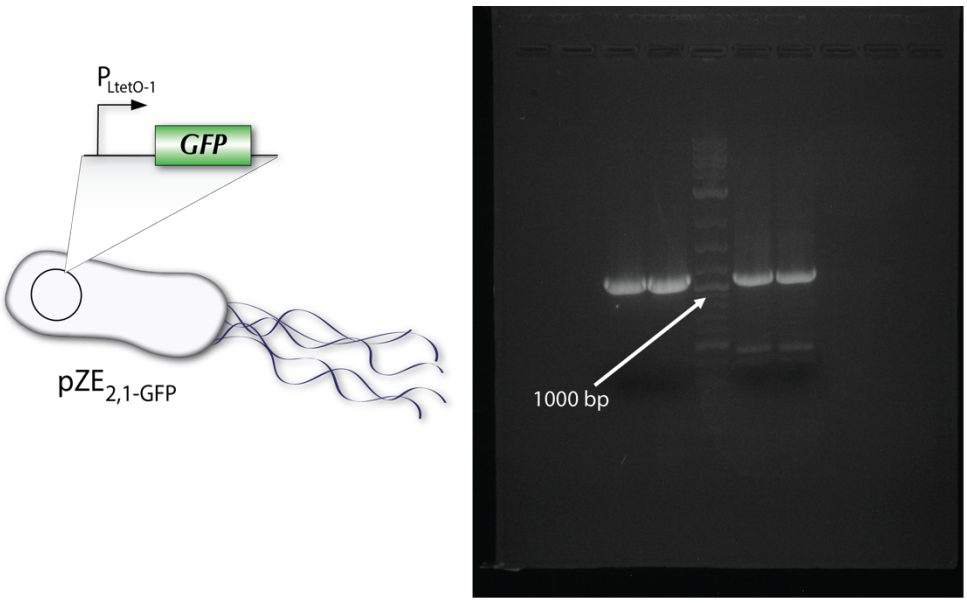

Figure 18: PCR product results. On the left is the synthetic circuit that was the objective of the PCR. On the right is the result of the gel electrophoresis confirming the correct size.

Figure 19 shows representative results from the imaging method used to collect the data in Figures 20-22. Notably, the green spheres are visible in both DIC and FITC contrasted images however

only the red fluorescent beads are visible in the TRITC image. These spheres allow for easy circular ROI's to be drawn on the images, making image analysis easier.

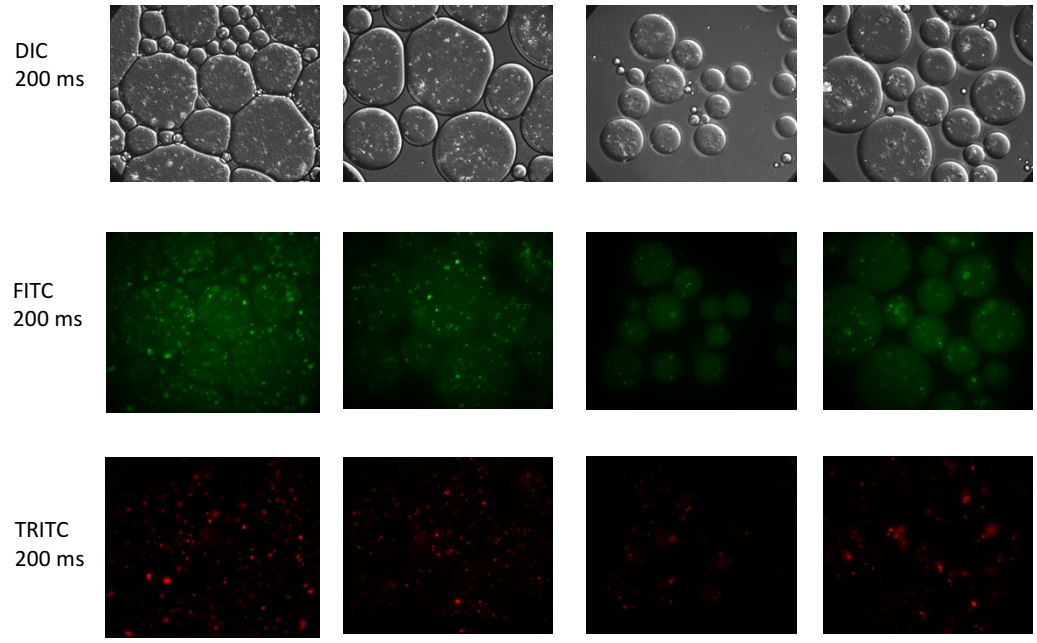

Figure 19: Representative results from imaging system for cell-free reactions. The top row shows DIC images taken with an exposure of 200 ms, the middle row contains FITC images with 200 ms exposure and the bottom row shows TRITC (red) images taken with 200 ms exposure time.

One would expect that in a cell free expression system, a higher concentration of DNA would result in higher protein expression, up until the maximum yield. With this in mind we set out to test the limits of our cell free expression system specifically with the biotinylated DNA produced. There is a clear trend (Figure X) between increasing the DNA concentration and measuring increased fluorescent intensity output. It is important to note that there is a small amount of fluorescent intensity with no DNA, and this should be accounted for when quantifying images in following experiments.

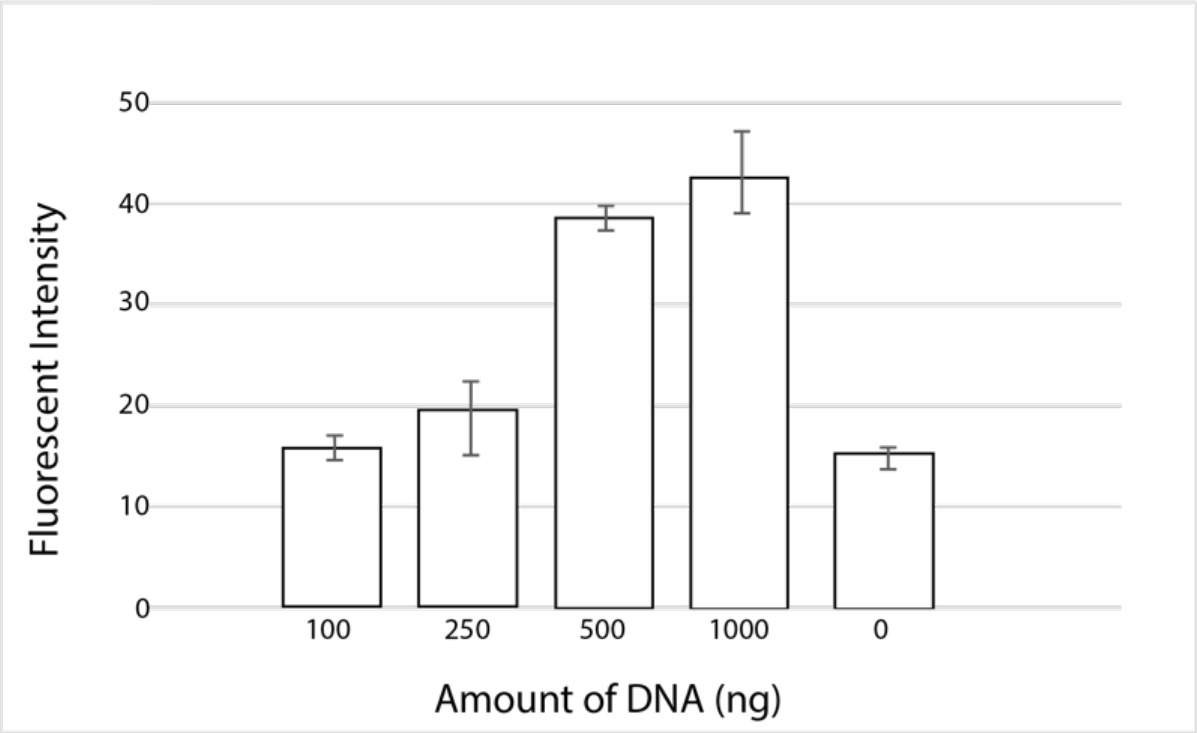

Figure 20: Effect of increasing DNA concentration on fluorescent intensity. As DNA concentration was increased we see an increase in the fluorescent intensity measured. Experiments were run in triplicate and standard deviation was calculated for each represented in the error bars shown.

By showing that our biotinylated DNA template can directly increase fluorescent intensity in cell free expression systems, we next set out to test the maximum DNA with the ability of microparticles to carry the DNA into the cell free system. Here we relied on the strong, non-covalent binding between biotin and SA. The biotinylated DNA, a biological component, was carried into the expression system after allowing time for interaction with a SA-functionalized microparticle. After measuring for fluorescent intensity of a varied number of microparticles with constant DNA (1 μg), we observe a distinct upward trend correlating increased microparticles and

fluorescent intensity. Since we previously showed that increased DNA concentration results in higher fluorescent intensity, we can now conclude that elevating the number of beads allows more DNA to enter the expression system, thereby resulting in a greater fluorescent intensity. We can additionally conclude that the interaction between the biotinylated DNA and SA-functionalized microparticles is strong and intact.

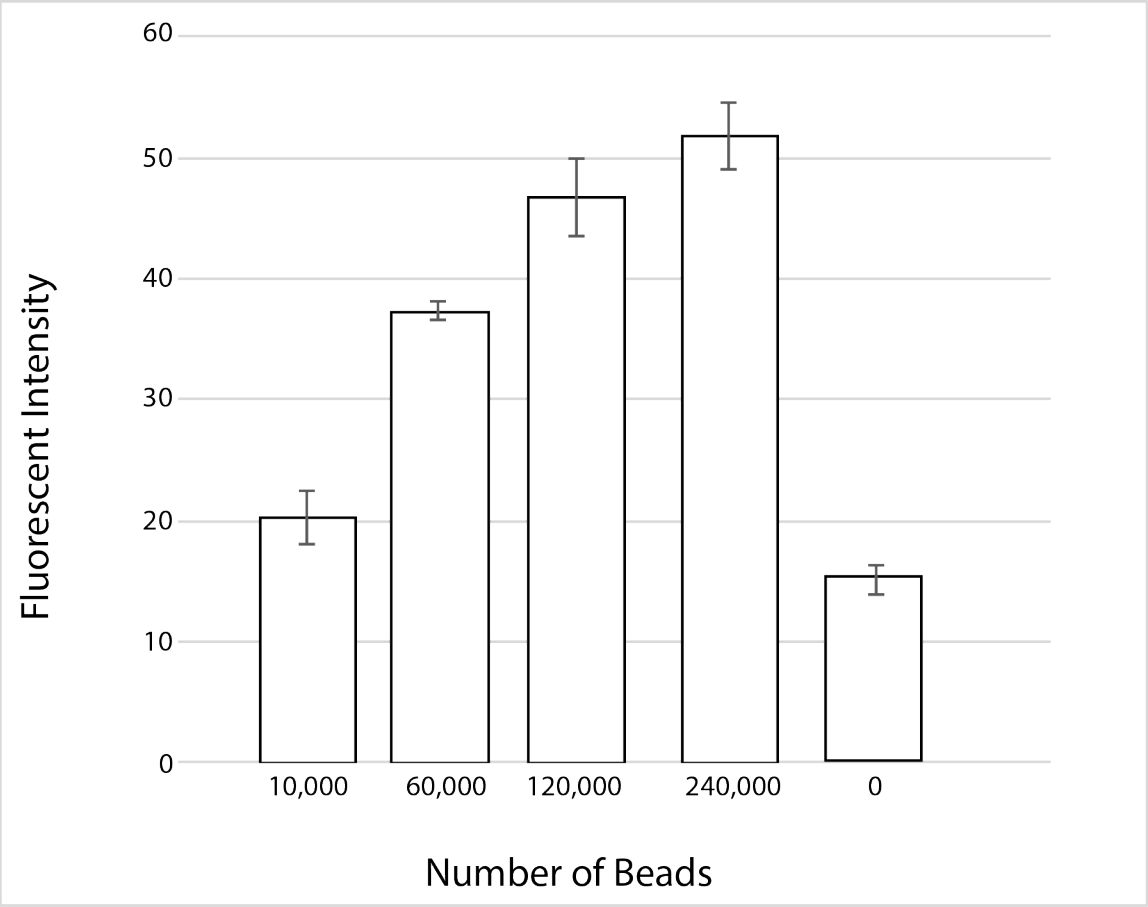

Figure 21: Increasing bead concentration's effect on fluorescent intensity. With an increase in the number of beads used in the system we see an increase in fluorescent intensity measured. This confirms the use of beads to carry the DNA template into the system. Experiments were run in triplicate with error bars showing standard deviation.

Lastly, we set out to test whether we can predictably modulate the fluorescent output with the addition of free biotin. We expect free biotin to competitively bind with biotinylated DNA for open SA places on the functionalized microparticles. Therefore, with the highest concentrations of free biotin, we expect to see the lowest fluorescent output and vice versa. In Figure X we see a large drop off in fluorescent intensity between 10 ng/mL and 100 ng/mL free biotin. There are small fluctuations but no appreciable difference between 100 ng/mL, 1000 ng/mL, 10000 ng/mL free biotin and the two controls. Control 1 (C1) is non-biotinylated DNA mixed with SA-functionalized beads. Control 2 (C2) has no DNA and is representative of the innate background fluorescence observed. Since C2 has a lower fluorescent output that C1, it seems there is a small amount of adsorption of the non-biotinylated DNA to the SA-functionalized nanoparticle. However, if we take the dynamic range of the system to be between 1-100 ng/mL free biotin, we can safely ignore any adsorption that would take place by non-biotinylated DNA.

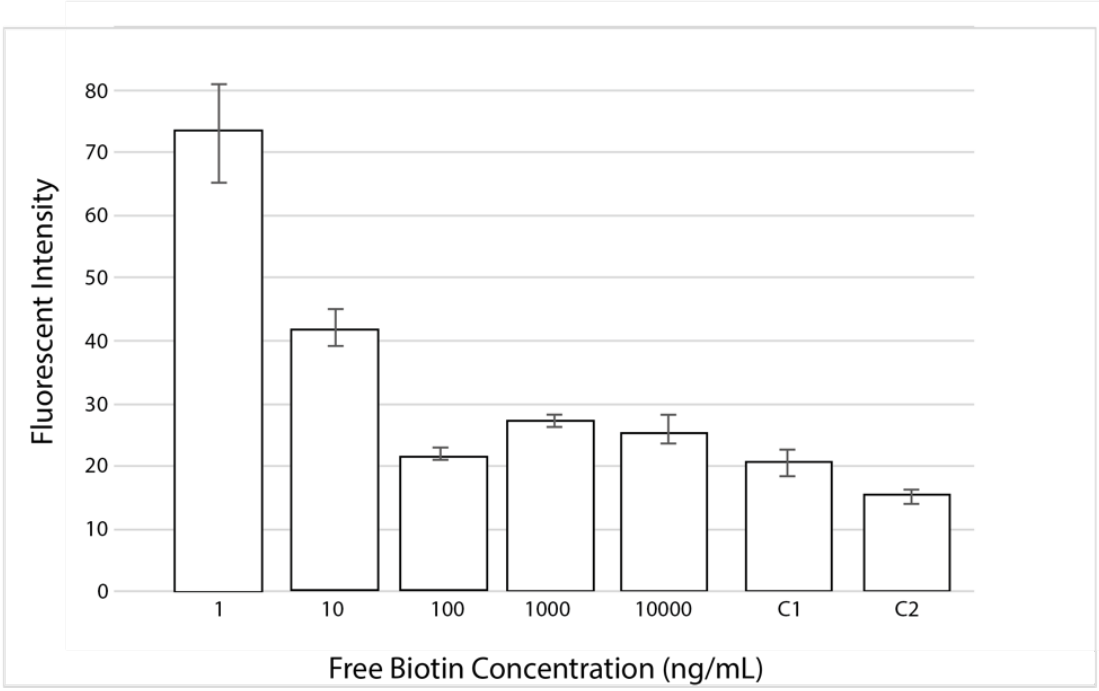

Figure 22: Free biotin modulates fluorescent intensity. By competitively binding with biotinylated DNA encoding GFP for binding sites on a streptavidin functionalized microparticle we are able to use free biotin to modulate a cell free expression system. Experiments were run in triplicate and standard deviations were calculated and shown as error bars on the graphs.

Conclusion

The system developed here, based on both living and non-living components, is capable of utilizing biological components for the output of a signaling protein, and of responding to molecules within its environment. We have shown the successful modulation of a cell free, transcription-translation, system using functionalized microparticles and biotinylated DNA. We believe this is a modular technology with the ability to quickly switch out different synthetic circuits or microparticle targeting for various applications within medicine and bioremediation.

Chapter VI: Conclusions and Future Work

Conclusions

In this thesis we have shown multiple enabling technologies for integrating biological components and microrobots for improved sensing and processing.

First we explored the use of the cell's surface as a means to spatially discretize synthetic circuit output. Crucially, the addition of a protein to the cell's outer surface, the SNAP-tag, capable of binding any BG modified constituents, allows the cell to serve as a sensor for extracellular molecules, anchor for the cell, or scaffold for agglomeration of multiple components. Next we studied information flow, through the transport of small molecules, between engineered bacteria and artificial protocells with encapsulated cell-free expression systems. Our results suggest linking these two simple systems can lead to complex circuitry behavior. Furthermore, we modeled a system capable of interacting with its environment and changing its protein expression based on input. Lastly, we experimentally modulated fluorescent protein expression with biological components using a microparticle scaffold. The ability to exploit biological components, readily available when traversing inside the body, is a key factor allowing for an essentially inexhaustible power source. For long term studies this would be crucial aspect reducing the need to retrieve a microrobotics device.

We believe we have created a robust processing unit of integrated biological and abiotic components capable of being deployed with a microrobotic system.

Future Work

Future work in the near future includes expanding the experimental results to include each system discussed in Chapter IV. Specifically, linking the biotin sensing system developed in Chapter V with engineered cells producing biotin and encapsulating the cell-free reaction within a liposomal

shell to create an artificial cell, similar to the ideas described in Chapter IV. Additionally, we would like to create a microfluidic chip that houses each of the separate components discussed (engineered cells, microparticles, cell-free expression).

References

[1] A. Rinaldi, "Naturally better. Science and technology are looking to nature's successful designs for inspiration," *EMBO Rep,* vol. 8, pp. 995-9, Nov 2007.

[2] I. Virgala, M. Kelemen, M. Varga, and P. Kuryło, "Analyzing, Modeling and Simulation of Humanoid Robot Hand Motion," *Procedia Engineering,* vol. 96, pp. 489-499, 2014/01/01 2014.

[3] S. Collins, A. Ruina, R. Tedrake, and M. Wisse, "Efficient Bipedal Robots Based on Passive-Dynamic Walkers," *Science,* vol. 307, p. 1082, 2005.

[4] A. L. Desbiens, Y. Chen, and R. J. Wood, "A wing characterization method for flapping-wing robotic insects," in *2013 IEEE/RSJ International Conference on Intelligent Robots and Systems*, 2013, pp. 1367-1373.

[5] B. M. Finio and R. J. Wood, "Open-loop roll, pitch and yaw torques for a robotic bee," in *2012 IEEE/RSJ International Conference on Intelligent Robots and Systems*, 2012, pp. 113-119.

[6] T. S. Gardner, C. R. Cantor, and J. J. Collins, "Construction of a genetic toggle switch in Escherichia coli," *Nature,* vol. 403, pp. 339-42, Jan 20 2000.

[7] A. A. Green, P. A. Silver, J. J. Collins, and P. Yin, "Toehold switches: de-novo-designed regulators of gene expression," *Cell,* vol. 159, pp. 925-39, Nov 06 2014.

[8] K. Pardee, A. A. Green, T. Ferrante, D. E. Cameron, A. DaleyKeyser, P. Yin*, et al.*, "Paper-based synthetic gene networks," *Cell,* vol. 159, pp. 940-54, Nov 06 2014.

[9] K. Pardee, A. A. Green, M. K. Takahashi, D. Braff, G. Lambert, J. W. Lee*, et al.*, "Rapid, Low-Cost Detection of Zika Virus Using Programmable Biomolecular Components," *Cell,* vol. 165, pp. 1255-66, May 19 2016.

[10] L. Royakkers and R. van Est, "A Literature Review on New Robotics: Automation from Love to War," *International Journal of Social Robotics,* vol. 7, pp. 549-570, 2015.

[11] A. J. Pearce, B. Adair, K. Miller, E. Ozanne, C. Said, N. Santamaria*, et al.*, "Robotics to enable older adults to remain living at home," *J Aging Res,* vol. 2012, p. 538169, 2012.

[12] W. Budiharto, "Intelligent Surveillance Robot with Obstacle Avoidance Capabilities Using Neural Network," *Comput Intell Neurosci,* vol. 2015, p. 745823, 2015.

[13] P. W. Singer, "Wired for war: The robotics revolution and conflict in the twenty-first century," ed: New York, NY: Penguin Books, 2009.

[14] C. G. Gourin and D. J. Terris, "Surgical robotics in otolaryngology: expanding the technology envelope," *Curr Opin Otolaryngol Head Neck Surg,* vol. 12, pp. 204-8, Jun 2004.

[15] R. M. Satava, "Surgical robotics: the early chronicles: a personal historical perspective," *Surg Laparosc Endosc Percutan Tech,* vol. 12, pp. 6-16, Feb 2002.

[16] A. van Wynsberghe, "Designing Robots for Care: Care Centered Value-Sensitive Design," *Science and Engineering Ethics,* vol. 19, pp. 407-433, 2013.

[17] I. O. f. Standardization, "Robots and robotic devices- vocabulary," in *ISO 8373:2012*, ed, 2012.

[18] D. Floreano and R. J. Wood, "Science, technology and the future of small autonomous drones," *Nature,* vol. 521, pp. 460-6, May 28 2015.

[19] W. J. Jack, "Microelectromechanical systems (MEMS): fabrication, design and applications," *Smart Materials and Structures,* vol. 10, p. 1115, 2001.
[20] A. Menciassi, M. Quirini, and P. Dario, "Microrobotics for future gastrointestinal endoscopy," *Minim Invasive Ther Allied Technol,* vol. 16, pp. 91-100, 2007.
[21] A. Koulaouzidis and S. Douglas, "Capsule endoscopy in clinical practice: concise up-to-date overview," *Clin Exp Gastroenterol,* vol. 2, pp. 111-6, 2009.
[22] B. J. Nelson, I. K. Kaliakatsos, and J. J. Abbott, "Microrobots for minimally invasive medicine," *Annu Rev Biomed Eng,* vol. 12, pp. 55-85, Aug 15 2010.
[23] M. Delvaux and G. Gay, "Capsule endoscopy: technique and indications," *Best Pract Res Clin Gastroenterol,* vol. 22, pp. 813-37, 2008.
[24] B. Behkam and M. Sitti, "Towards Hybrid Swimming Microrobots: Bacteria Assisted Propulsion of Polystyrene Beads," in *2006 International Conference of the IEEE Engineering in Medicine and Biology Society*, 2006, pp. 2421-2424.
[25] M. A. Traore and B. Behkam, "A stochastic model for chemotactic motion of micro-beads propelled by attached bacteria," in *2010 3rd IEEE RAS & EMBS International Conference on Biomedical Robotics and Biomechatronics*, 2010, pp. 704-709.
[26] M. A. Traoré, A. Sahari, and B. Behkam, "Computational and experimental study of chemotaxis of an ensemble of bacteria attached to a microbead," *Physical Review E,* vol. 84, p. 061908, 12/12/ 2011.
[27] S. Cho, Y. J. Choi, S. Zheng, J. Han, S. Y. Ko, J. O. Park*, et al.*, "Modeling of chemotactic steering of bacteria-based microrobot using a population-scale approach," *Biomicrofluidics,* vol. 9, p. 054116, Sep 2015.
[28] A. Sahari, D. Headen, and B. Behkam, "Effect of body shape on the motile behavior of bacteria-powered swimming microrobots (BacteriaBots)," *Biomed Microdevices,* vol. 14, pp. 999-1007, Dec 2012.
[29] Q. Ma, C. Chen, S. Wei, C. Chen, L. F. Wu, and T. Song, "Construction and operation of a microrobot based on magnetotactic bacteria in a microfluidic chip," *Biomicrofluidics,* vol. 6, pp. 24107-2410712, Jun 2012.
[30] E. Steager, C.-B. Kim, J. Patel, S. Bith, C. Naik, L. Reber*, et al.*, "Control of microfabricated structures powered by flagellated bacteria using phototaxis," *Applied Physics Letters,* vol. 90, p. 263901, 2007.
[31] V. Chan, K. Park, M. B. Collens, H. Kong, T. A. Saif, and R. Bashir, "Development of Miniaturized Walking Biological Machines," *Scientific Reports,* vol. 2, p. 857, 11/15/online 2012.
[32] R. D. Kamm and R. Bashir, "Creating living machines," *Annals of biomedical engineering,* vol. 42, pp. 445-459, 09/05 2014.
[33] R. Raman, C. Cvetkovic, S. G. M. Uzel, R. J. Platt, P. Sengupta, R. D. Kamm*, et al.*, "Optogenetic skeletal muscle-powered adaptive biological machines," *Proceedings of the National Academy of Sciences,* vol. 113, pp. 3497-3502, March 29, 2016 2016.
[34] S. J. Park, M. Gazzola, K. S. Park, S. Park, V. Di Santo, E. L. Blevins*, et al.*, "Phototactic guidance of a tissue-engineered soft-robotic ray," *Science,* vol. 353, pp. 158-62, Jul 08 2016.
[35] M. B. Elowitz and S. Leibler, "A synthetic oscillatory network of transcriptional regulators," *Nature,* vol. 403, pp. 335-8, Jan 20 2000.

[36] A. E. Friedland, T. K. Lu, X. Wang, D. Shi, G. Church, and J. J. Collins, "Synthetic gene networks that count," *Science,* vol. 324, pp. 1199-202, May 29 2009.
[37] J. C. Anderson, C. A. Voigt, and A. P. Arkin, "Environmental signal integration by a modular AND gate," *Mol Syst Biol,* vol. 3, p. 133, 2007.
[38] T. Ellis, X. Wang, and J. J. Collins, "Diversity-based, model-guided construction of synthetic gene networks with predicted functions," *Nat Biotechnol,* vol. 27, pp. 465-71, May 2009.
[39] B. Xia, S. Bhatia, B. Bubenheim, M. Dadgar, D. Densmore, and J. C. Anderson, "Developer's and user's guide to Clotho v2.0 A software platform for the creation of synthetic biological systems," *Methods Enzymol,* vol. 498, pp. 97-135, 2011.
[40] L. Bilitchenko, A. Liu, S. Cheung, E. Weeding, B. Xia, M. Leguia*, et al.*, "Eugene--a domain specific language for specifying and constraining synthetic biological parts, devices, and systems," *PloS one,* vol. 6, p. e18882, 2011.
[41] C. Sanchez, H. Arribart, and M. M. Guille, "Biomimetism and bioinspiration as tools for the design of innovative materials and systems," *Nat Mater,* vol. 4, pp. 277-88, Apr 2005.
[42] Z. Xie, L. Wroblewska, L. Prochazka, R. Weiss, and Y. Benenson, "Multi-input RNAi-based logic circuit for identification of specific cancer cells," *Science,* vol. 333, pp. 1307-11, Sep 2 2011.
[43] K. Rinaudo, L. Bleris, R. Maddamsetti, S. Subramanian, R. Weiss, and Y. Benenson, "A universal RNAi-based logic evaluator that operates in mammalian cells," *Nat Biotechnol,* vol. 25, pp. 795-801, Jul 2007.
[44] A. Tamsir, J. J. Tabor, and C. A. Voigt, "Robust multicellular computing using genetically encoded NOR gates and chemical 'wires'," *Nature,* vol. 469, pp. 212-5, Jan 13 2011.
[45] J. Bonnet, P. Subsoontorn, and D. Endy, "Rewritable digital data storage in live cells via engineered control of recombination directionality," *Proc Natl Acad Sci U S A,* vol. 109, pp. 8884-9, Jun 5 2012.
[46] P. Siuti, J. Yazbek, and T. K. Lu, "Synthetic circuits integrating logic and memory in living cells," *Nat Biotechnol,* vol. 31, pp. 448-52, May 2013.
[47] R. Daniel, J. R. Rubens, R. Sarpeshkar, and T. K. Lu, "Synthetic analog computation in living cells," *Nature,* vol. 497, pp. 619-23, May 30 2013.
[48] M. K. Rice and W. C. Ruder, "Creating biological nanomaterials using synthetic biology," *Sci Technol Adv Mater,* vol. 15, p. 014401, Feb 2014.
[49] M. B. Hoagland, M. L. Stephenson, J. F. Scott, L. I. Hecht, and P. C. Zamecnik, "A soluble ribonucleic acid intermediate in protein synthesis," *J Biol Chem,* vol. 231, pp. 241-57, Mar 1958.
[50] G. Zubay, "In vitro synthesis of protein in microbial systems," *Annu Rev Genet,* vol. 7, pp. 267-87, 1973.
[51] S. Tabor and C. C. Richardson, "A bacteriophage T7 RNA polymerase/promoter system for controlled exclusive expression of specific genes," *Proc Natl Acad Sci U S A,* vol. 82, pp. 1074-8, Feb 1985.
[52] J. Shin and V. Noireaux, "Study of messenger RNA inactivation and protein degradation in an Escherichia coli cell-free expression system," *J Biol Eng,* vol. 4, p. 9, Jul 01 2010.

[53] M. B. Iskakova, W. Szaflarski, M. Dreyfus, J. Remme, and K. H. Nierhaus, "Troubleshooting coupled in vitro transcription-translation system derived from Escherichia coli cells: synthesis of high-yield fully active proteins," *Nucleic Acids Res,* vol. 34, p. e135, 2006.

[54] T. Kigawa, T. Yabuki, N. Matsuda, T. Matsuda, R. Nakajima, A. Tanaka*, et al.*, "Preparation of Escherichia coli cell extract for highly productive cell-free protein expression," *J Struct Funct Genomics,* vol. 5, pp. 63-8, 2004.

[55] Z. Z. Sun, C. A. Hayes, J. Shin, F. Caschera, R. M. Murray, and V. Noireaux, "Protocols for implementing an Escherichia coli based TX-TL cell-free expression system for synthetic biology," *J Vis Exp,* p. e50762, 2013.

[56] C. E. Hodgman and M. C. Jewett, "Cell-free synthetic biology: thinking outside the cell," *Metab Eng,* vol. 14, pp. 261-9, May 2012.

[57] K. Pardee, S. Slomovic, P. Q. Nguyen, J. W. Lee, N. Donghia, D. Burrill*, et al.*, "Portable, On-Demand Biomolecular Manufacturing," *Cell,* vol. 167, pp. 248-259 e12, Sep 22 2016.

[58] M. R. Bennett, W. L. Pang, N. A. Ostroff, B. L. Baumgartner, S. Nayak, L. S. Tsimring*, et al.*, "Metabolic gene regulation in a dynamically changing environment," *Nature,* vol. 454, pp. 1119-22, Aug 28 2008.

[59] J. Stricker, S. Cookson, M. R. Bennett, W. H. Mather, L. S. Tsimring, and J. Hasty, "A fast, robust and tunable synthetic gene oscillator," *Nature,* vol. 456, pp. 516-519, 11/27/print 2008.

[60] D. Irimia, G. Balázsi, N. Agrawal, and M. Toner, "Adaptive-Control Model for Neutrophil Orientation in the Direction of Chemical Gradients," *Biophysical Journal,* vol. 96, pp. 3897-3916, 5/20/ 2009.

[61] A. Pai, Y. Tanouchi, and L. You, "Optimality and robustness in quorum sensing (QS)-mediated regulation of a costly public good enzyme," *Proceedings of the National Academy of Sciences,* vol. 109, pp. 19810-19815, 2012.

[62] L. You, R. S. Cox, R. Weiss, and F. H. Arnold, "Programmed population control by cell-cell communication and regulated killing," *Nature,* vol. 428, pp. 868-871, 04/22/print 2004.

[63] F. Y. Scott, K. C. Heyde, M. K. Rice, and W. C. Ruder, "Spatial segregation of synthetic circuit output using the cell surface," *OUP Synthetic Biology,* submitted 2017.

[64] P. Samuelson, E. Gunneriusson, P.-A. Nygren, and S. Stahl, "Display of Proteins on Bacteria," *Journal of Biotechnology,* vol. 96, pp. 129-154, 2002.

[65] A. Keppler, S. Gendreizig, T. Gronemeyer, H. Pick, H. Vogel, and K. Johnsson, "A general method for the covalent labeling of fusion proteins with small molecules in vivo," *Nature Biotechnology,* vol. 21, pp. 86-9, Jan 2003
2013-02-05 2003.

[66] T. Gronemeyer, C. Chidley, A. Juillerat, C. Heinis, and K. Johnsson, "Directed evolution of O6-alkylguanine-DNA alkyltransferase for applications in protein labeling," *Protein Engineering, Design and Selection,* vol. 19, pp. 309-16, Jul 2006.

[67] F. Kampmeier, J. Niesen, A. Koers, M. Ribbert, A. Brecht, R. Fischer*, et al.*, "Rapid optical imaging of EGF receptor expression with a single-chain antibody SNAP-tag fusion protein," *European Journal of Nuclear Medicine and Molecular Imaging,* vol. 37, pp. 1926-1934, 2010/10/01 2010.

[68] A. Pardo, M. Stöcker, F. Kampmeier, G. Melmer, R. Fischer, T. Thepen*, et al.*, "In vivo imaging of immunotoxin treatment using Katushka-transfected A-431 cells in a murine xenograft tumour model," *Cancer Immunology, Immunotherapy,* vol. 61, pp. 1617-1626, 2012/10/01 2012.

[69] A. F. Hussain, F. Kampmeier, V. von Felbert, H.-F. Merk, M. K. Tur, and S. Barth, "SNAP-Tag Technology Mediates Site Specific Conjugation of Antibody Fragments with a Photosensitizer and Improves Target Specific Phototoxicity in Tumor Cells," *Bioconjugate Chemistry,* vol. 22, pp. 2487-2495, 2011/12/21 2011.

[70] C. Jing and V. W. Cornish, "Chemical Tags for Labeling Proteins Inside Living Cells," *Accounts of Chemical Research,* vol. 44, pp. 784-792, 2011/09/20 2011.

[71] D. Srikun, A. E. Albers, C. I. Nam, A. T. Iavarone, and C. J. Chang, "Organelle-Targetable Fluorescent Probes for Imaging Hydrogen Peroxide in Living Cells via SNAP-Tag Protein Labeling," *Journal of the American Chemical Society,* vol. 132, pp. 4455-4465, 2010/03/31 2010.

[72] C. E. Chivers, A. L. Koner, E. D. Lowe, and M. Howarth, "How the biotin-streptavidin interaction was made even stronger: investigation via crystallography and a chimaeric tetramer," *Biochem J,* vol. 435, pp. 55-63, Apr 01 2011.

[73] K. Stohr, D. Siegberg, T. Ehrhard, K. Lymperopoulos, S. Oz, S. Schulmeister*, et al.*, "Quenched Substrates for Live-Cell Labeling of SNAP-Tagged Fusion Proteins with Improved Fluorescent Background," *Analytical Chemistry,* vol. 82, pp. 8186-8193, 2010.

[74] T. Baba, T. Ara, M. Hasegawa, Y. Takai, Y. Okumura, M. Baba*, et al.*, "Construction of Escherichia coli K-12 in-frame, single-gene knockout mutants: the Keio collection," *Molecular Systems Biology,* vol. 2, 2006-01-01 00:00:00 2006.

[75] K. Kolberg, C. Puettmann, A. Pardo, J. Fitting, and S. Barth, "SNAP-Tag Technology: A General Introduction," *Current Pharmaceutical Design,* vol. 19, pp. 5406-5413, 2013.

[76] Y. Shimizu, A. Inoue, Y. Tomari, T. Suzuki, T. Yokogawa, K. Nishikawa*, et al.*, "Cell-free translation reconstituted with purified components," *Nat Biotechnol,* vol. 19, pp. 751-5, Aug 2001.

[77] E. Karzbrun, A. M. Tayar, V. Noireaux, and R. H. Bar-Ziv, "Synthetic biology. Programmable on-chip DNA compartments as artificial cells," *Science,* vol. 345, pp. 829-32, Aug 15 2014.

[78] C. Tan, S. Saurabh, M. P. Bruchez, R. Schwartz, and P. Leduc, "Molecular crowding shapes gene expression in synthetic cellular nanosystems," *Nat Nanotechnol,* vol. 8, pp. 602-8, Aug 2013.

[79] V. Noireaux, Y. T. Maeda, and A. Libchaber, "Development of an artificial cell, from self-organization to computation and self-reproduction," *Proc Natl Acad Sci U S A,* vol. 108, pp. 3473-80, Mar 1 2011.

[80] H. M. Said, "Cell and molecular aspects of human intestinal biotin absorption," *J Nutr,* vol. 139, pp. 158-62, Jan 2009.

[81] H. G. Wood and R. E. Barden, "Biotin enzymes," *Annu Rev Biochem,* vol. 46, pp. 385-413, 1977.

[82] K. C. Heyde, M. K. Rice, S.-H. Paek, F. Y. Scott, R. Zhang, and W. C. Ruder, "Modeling information exchange between living and artificial cells," *Quantitative Biology,* vol. 5, pp. 76-89, 2017.

[83] K. C. Heyde and W. C. Ruder, "Exploring Host-Microbiome Interactions using an in Silico Model of Biomimetic Robots and Engineered Living Cells," *Scientific Reports,* vol. 5, p. 11988, 07/16/online 2015.
[84] K. C. Heyde, P. W. Gallagher, and W. C. Ruder, "Bioinspired decision architectures containing host and microbiome processing units," *Bioinspiration & Biomimetics,* vol. 11, p. 056017, 2016.
[85] R. Zhang, K. C. Heyde, F. Y. Scott, S.-H. Paek, and W. C. Ruder, "Programming Surface Chemistry with Engineered Cells," *ACS Synthetic Biology,* 2016/05/20 2016.
[86] J. Garcia-Ojalvo, M. B. Elowitz, and S. H. Strogatz, "Modeling a synthetic multicellular clock: Repressilators coupled by quorum sensing," *Proceedings of the National Academy of Sciences of the United States of America,* vol. 101, pp. 10955-10960, July 27, 2004 2004.
[87] T. Stogbauer, L. Windhager, R. Zimmer, and J. O. Radler, "Experiment and mathematical modeling of gene expression dynamics in a cell-free system," *Integrative Biology,* vol. 4, pp. 494-501, 2012.
[88] P. Weber, D. Ohlendorf, J. Wendoloski, and F. Salemme, "Structural origins of high-affinity biotin binding to streptavidin," *Science,* vol. 243, pp. 85-88, January 6, 1989 1989.
[89] H. Tran, S. M. D. Oliveira, N. Goncalves, and A. S. Ribeiro, "Kinetics of the cellular intake of a gene expression inducer at high concentrations," *Molecular BioSystems,* vol. 11, pp. 2579-2587, 2015.
[90] H. Xu, M. Moraitis, R. J. Reedstrom, and K. S. Matthews, "Kinetic and Thermodynamic Studies of Purine Repressor Binding to Corepressor and Operator DNA," *Journal of Biological Chemistry,* vol. 273, pp. 8958-8964, April 10, 1998 1998.
[91] N. Politi, L. Pasotti, S. Zucca, M. Casanova, G. Micoli, M. G. Cusella De Angelis*, et al.*, "Half-life measurements of chemical inducers for recombinant gene expression," *Journal of Biological Engineering,* vol. 8, p. 5, 2014.
[92] N. M. Green, "Avidin. 3. The nature of the biotin-binding site," *Biochemical Journal,* vol. 89, pp. 599-609, 1963.
[93] S.-C. Huang, M. D. Stump, R. Weiss, and K. D. Caldwell, "Binding of Biotinylated DNA to Streptavidin-Coated Polystyrene Latex: Effects of Chain Length and Particle Size," *Analytical Biochemistry,* vol. 237, pp. 115-122, 1996/05/15 1996.
[94] V. Noireaux, R. Bar-Ziv, and A. Libchaber, "Principles of cell-free genetic circuit assembly," *Proceedings of the National Academy of Sciences,* vol. 100, pp. 12672-12677, October 28, 2003 2003.
[95] S. S. Daube and R. H. Bar-Ziv, "Protein nanomachines assembly modes: cell-free expression and biochip perspectives," *Wiley Interdisciplinary Reviews: Nanomedicine and Nanobiotechnology,* vol. 5, pp. 613-628, 2013.
[96] A. Groisman, C. Lobo, H. Cho, J. K. Campbell, Y. S. Dufour, A. M. Stevens*, et al.*, "A microfluidic chemostat for experiments with bacterial and yeast cells," *Nat Meth,* vol. 2, pp. 685-689, 09//print 2005.
[97] F. J. H. Hol and C. Dekker, "Zooming in to see the bigger picture: Microfluidic and nanofabrication tools to study bacteria," *Science,* vol. 346, 2014.

[98] Z. Z. Sun, C. A. Hayes, J. Shin, F. Caschera, R. M. Murray, and V. Noireaux, "Protocols for Implementing an Escherichia coli Based TX-TL Cell-Free Expression System for Synthetic Biology," p. e50762, 2013/09/16/ 2013.
[99] R. Lutz and H. Bujard, "Independent and Tight Regulation of Transcriptional Units in Escherichia Coli Via the LacR/O, the TetR/O and AraC/I1-I2 Regulatory Elements," *Nucleic Acids Research,* vol. 25, pp. 1203-1210, March 1, 1997 1997.
[100] I. Sanyal, G. Cohen, and D. H. Flint, "Biotin Synthase: Purification, Characterization as a [2Fe-2S]Cluster Protein, and in vitro Activity of the Escherichia coli bioB Gene Product," *Biochemistry,* vol. 33, pp. 3625-3631, 1994/03/01 1994.
[101] J. A. N. Brophy and C. A. Voigt, "Principles of genetic circuit design," *Nat Meth,* vol. 11, pp. 508-520, 05//print 2014.
[102] J. C. Anderson, C. A. Voigt, and A. P. Arkin, "Environmental signal integration by a modular AND gate," *Molecular Systems Biology,* vol. 3, 2007.
[103] D. E. Cameron and J. J. Collins, "Tunable protein degradation in bacteria," *Nat Biotech,* vol. 32, pp. 1276-1281, 12//print 2014.
[104] T. S. Gardner, C. R. Cantor, and J. J. Collins, "Construction of a genetic toggle switch in Escherichia coli," *Nature,* vol. 403, pp. 339-342, 01/20/print 2000.
[105] K. A. Johnson and R. S. Goody, "The Original Michaelis Constant: Translation of the 1913 Michaelis–Menten Paper," *Biochemistry,* vol. 50, pp. 8264-8269, 2011/10/04 2011.
[106] M. González, L. A. Bagatolli, I. Echabe, J. L. R. Arrondo, C. E. Argaraña, C. R. Cantor*, et al.*, "Interaction of Biotin with Streptavidin: THERMOSTABILITY AND CONFORMATIONAL CHANGES UPON BINDING," *Journal of Biological Chemistry,* vol. 272, pp. 11288-11294, April 25, 1997 1997.
[107] M. Schwarz-Schilling, L. Aufinger, A. Muckl, and F. C. Simmel, "Chemical communication between bacteria and cell-free gene expression systems within linear chains of emulsion droplets," *Integrative Biology,* vol. 8, pp. 564-570, 2016.
[108] K. Brenner, L. You, and F. H. Arnold, "Engineering microbial consortia: a new frontier in synthetic biology," *Trends Biotechnol,* vol. 26, pp. 483-9, Sep 2008.
[109] S. G. Hays, W. G. Patrick, M. Ziesack, N. Oxman, and P. A. Silver, "Better together: engineering and application of microbial symbioses," *Curr Opin Biotechnol,* vol. 36, pp. 40-9, Dec 2015.
[110] E. H. Wintermute and P. A. Silver, "Dynamics in the mixed microbial concourse," *Genes Dev,* vol. 24, pp. 2603-14, Dec 1 2010.
[111] F. K. Balagadde, H. Song, J. Ozaki, C. H. Collins, M. Barnet, F. H. Arnold*, et al.*, "A synthetic Escherichia coli predator-prey ecosystem," *Mol Syst Biol,* vol. 4, p. 187, 2008.
[112] Z. Z. Sun, C. A. Hayes, J. Shin, F. Caschera, R. M. Murray, and V. Noireaux, "Protocols for Implementing an Escherichia coli Based TX-TL Cell-Free Expression System for Synthetic Biology," *Journal of Visualized Experiments : JoVE,* p. 50762, 09/16 2013.